

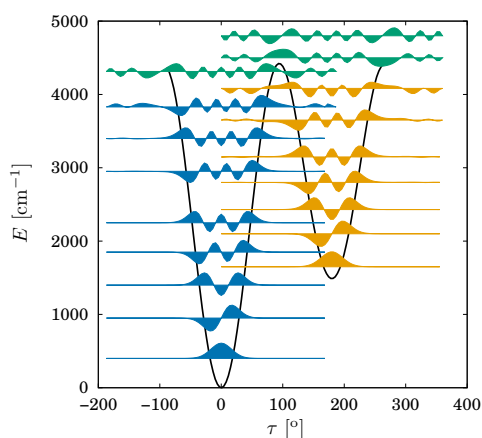
# Variational vibrational states of HCOOH

Alberto Martín Santa Daría,<sup>1</sup> Gustavo Avila,<sup>1,\*</sup> and Edit Mátyus<sup>1,†</sup>

<sup>1</sup>*ELTE, Eötvös Loránd University, Institute of Chemistry,  
Pázmány Péter sétány 1/A, 1117 Budapest, Hungary*

(Dated: 11 March 2022)

Vibrational states of the formic acid molecule are converged using the GENIUSH–Smolyak approach and the potential energy surface taken from [D. Tew and W. Mizukami, J. Phys. Chem. A 120, 9815 (2016)]. The quantum nuclear motion is described by using the *cis-trans* torsional coordinate and eight curvilinear normal coordinates defined with respect to an instantaneous reference configuration changing as a function of the torsional degree of freedom. Harmonic oscillator basis functions are used for the curvilinear normal coordinates, a Fourier basis for the torsional coordinate, and a simple basis pruning condition is combined with a Smolyak integration grid. *Trans*, *cis*, and *delocalized* vibrational states are reported up to and slightly beyond the isomerization barrier.



\* [Gustavo\\_Avila@telefonica.net](mailto:Gustavo_Avila@telefonica.net)

† [edit.matyus@ttk.elte.hu](mailto:edit.matyus@ttk.elte.hu)

## I. INTRODUCTION

This paper is dedicated to the memory of J. K. G. Watson, the father of the Watson Hamiltonian, a compact, analytic formulation of the rovibrational kinetic energy operator in normal coordinates. In this paper, we also use normal coordinates, but we adapt these coordinates to the *cis-trans* isomerization of the formic acid molecule. There is no known analytic formulation for the corresponding kinetic energy operator available, and we use computer power to construct the kinetic energy coefficients where they are needed.

Over the past decade, we have observed a rapid and fundamentally important development of exact quantum dynamics techniques to solve the (ro)vibrational problem. Development is observed in several directions: (a) coordinate representation and the kinetic energy operator [1–7]; (b) contraction techniques [8–12]; (c) grid pruning techniques [13–18]; (d) collocation [19–21]; (e) accurate potential energy representations for high-dimensional systems [22–24]; (f) highly parallel computation of ten thousands or millions of vibrational states [25–27].

Regarding the formic acid molecule, there are two full-dimensional, high-level *ab initio* potential energy surfaces (PESs) [28, 29] that have been used in sophisticated (variational or perturbative) vibrational computations. Tew and Mizukami used their PES in a variational vibrational computation with a five-mode representation and the internal-coordinate path Hamiltonian (ICPH) approach [28]. Richter and Carbonnière used a similar PES [29], computed vibrational energies using a valence-coordinate representation of the kinetic energy operator and the multi-configuration time-dependent Hartree approach, and they reported significant deviations from Ref. [28] for the vibrational states of the *cis* potential energy well. Last year, Nejad and Sibert used both PESs and sixth-order canonical Van Vleck perturbation theory (CVPT) in curvilinear normal coordinates localized in one of the potential energy wells (*trans* or *cis*) of the molecule [30].

In the present work, we focus on the vibrational methodology and define an efficient setup that can be used to converge (better than  $5\text{ cm}^{-1}$ ) all vibrational states of the formic acid molecule up to and possibly beyond the isomerization barrier. During the course of the development of a benchmark-quality variational vibrational setup, we use the Tew–Mizukami PES [28] (henceforth labelled as TM16-PES). It is left for future work, when well-converged vibrational energies can be ‘routinely’ computed for the relevant energy range of this system, to decide which PES representation performs better in comparison with experiment (gas-phase overtone and combination bands). Vibrational band origins are available from experimental infrared and Raman observations, a review and an extensive list of references can be found in the introduction of Ref. [30].

The present work is organized as follows. Sec. II reports the development of a torsional-curvilinear normal coordinate representation. Sec. III describes the construction of the corresponding kinetic energy operator coefficients using the numerical kinetic energy operator approach as it is implemented in the GENIUSH computer program [2]. Sec. IV defines the harmonic oscillator basis functions for the curvilinear normal coordinates, the Fourier basis and torsional functions for the torsional degree of freedom, and discusses basis pruning strategies. Sec. V describes the Smolyak non-product grid technique that is used to compute multi-dimensional integrals. In Sec. VI, vibrational energies are presented and discussed in relation with earlier computations [28, 30], and further necessary development and computational work is outlined.

## II. VIBRATIONAL COORDINATES

### A. Internal coordinates

The body-fixed Cartesian coordinates of HCOOH are defined in terms of the  $r_i \in [0, \infty)$  distances, the  $\theta_i \in [0, \pi]$  angles, the  $\varphi \in [-\pi, \pi)$  out-of-plane bending, and the  $\tau \in [0, 2\pi)$  torsional angle

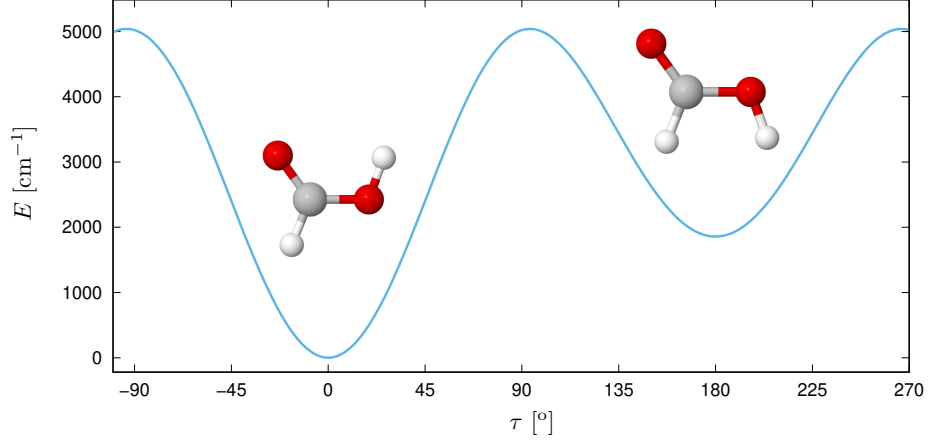


FIG. 1. 1-dimensional cut of the TM16-PES [28] along the torsional angle ( $\tau$ ) that describes the conversion between the *trans* and the *cis* conformers of the formic acid molecule.

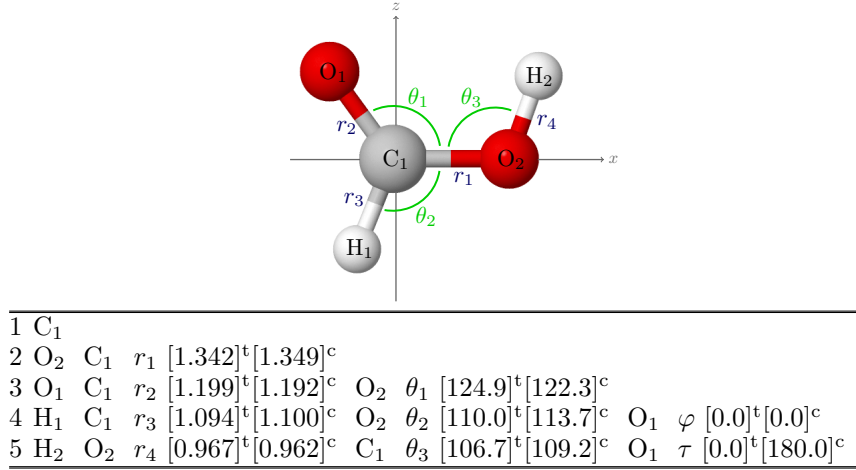


FIG. 2. Visualization of the internal coordinates, Eq. (1), for the example of the *trans*-formic acid molecule in its equilibrium structure. The equilibrium values of the distances, in Å and the angles, in degree, corresponding to the *cis* (°) and the *trans* (°) conformers on the TM16-PES are shown in brackets.

according to the following expressions:

$$\begin{aligned}
 \mathbf{r}_{C_1} &= \mathbf{0}, \quad \mathbf{r}_{O_2} = \begin{pmatrix} 0 \\ 0 \\ r_1 \end{pmatrix}, \quad \mathbf{r}_{O_1} = \begin{pmatrix} 0 \\ r_2 \cos(\theta_1 - \pi/2) \\ -r_2 \sin(\theta_1 - \pi/2) \end{pmatrix}, \\
 \mathbf{r}_{H_1} &= \begin{pmatrix} r_3 \cos(\theta_2 - \pi/2) \sin \varphi \\ -r_3 \cos(\theta_2 - \pi/2) \cos \varphi \\ -r_3 \sin(\theta_2 - \pi/2) \end{pmatrix}, \quad \mathbf{r}_{H_2} = \mathbf{r}_{O_2} + \begin{pmatrix} r_4 \cos(\theta_3 - \pi/2) \sin \tau \\ r_4 \cos(\theta_3 - \pi/2) \cos \tau \\ r_4 \sin(\theta_3 - \pi/2) \end{pmatrix}.
 \end{aligned} \tag{1}$$

The coordinate definition and the corresponding  $Z$ -matrix including the equilibrium values at the *trans* and the *cis* minima of the TM16-PES are summarized in Figure 2. For later use, a compact notation of the coordinates is introduced as

$$\boldsymbol{\xi} = (\xi_1, \dots, \xi_9) = (r_1, r_2, r_3, r_4, \theta_1, \theta_2, \theta_3, \varphi, \tau). \tag{2}$$

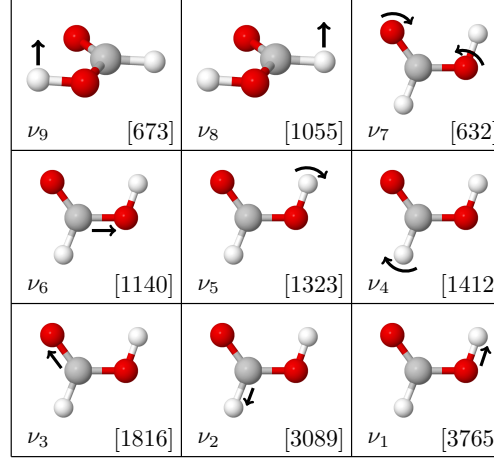


FIG. 3. Visualization of the normal modes corresponding to the global minimum (*trans*) of HCOOH. The harmonic frequencies, in  $\text{cm}^{-1}$ , are shown in brackets.

### B. Rectilinear normal coordinates

The body-fixed Cartesian coordinates and displacements with respect to the  $c_{i\alpha}$  reference (equilibrium) geometry of an  $N$ -atomic molecule can be written in terms of the  $Q_k \in \mathbb{R}$  normal coordinates as

$$r_{i\alpha} = c_{i\alpha} + d_{i\alpha} \quad \text{with} \quad d_{i\alpha} = \frac{1}{m_i^{1/2}} \sum_{k=1}^{\bar{D}} l_{i\alpha,k} Q_k, \quad i = 1, \dots, N, \quad \text{and } \alpha = x, y, z. \quad (3)$$

The  $l_{i\alpha,k}$  coefficients are the elements of the eigenvectors of the  $\mathbf{GF}$  matrix [31] evaluated at the reference (equilibrium) structure. In this work, the normal coordinate calculation has been performed at both minima (*trans* and *cis*) of HCOOH, hence, there are two parameter sets. The  $\mathbf{F}$  Hessian matrix has been computed by finite differences of the PES at both (*trans* and *cis*) equilibrium structures with respect to the displacements along the  $3N$  Cartesian coordinates. The numerical derivatives and related mathematical manipulations were evaluated using the Wolfram Mathematica symbolic algebra program [32].

HCOOH is an  $N = 5$ -atomic molecule and its total number of vibrational degrees of freedom is  $3N - 6 = 9$ . We used Eq. (3) with  $\bar{D} = 9$  (Fig. 3), but we also used it with  $\bar{D} = 8$  while the  $\tau$  torsional degree of freedom was excluded from the harmonic analysis that is necessary to have a good description for the *cis-trans* isomerization.

### C. Curvilinear normal coordinates

Instead of using rectilinear displacement coordinates,  $d_{i\alpha}$ , a better vibrational representation can be obtained [33], if we use (curvilinear) internal coordinates (Fig. 2), for which curvilinear displacement (c-displacement) coordinates can be defined with respect to some reference (equilibrium, eq) value as

$$\Delta\xi_i = \xi_i - \xi_i^{(\text{eq})}. \quad (4)$$

We define linear combinations of these curvilinear displacement coordinates, and we call them curvilinear (c-normal) normal coordinates,

$$\mathcal{Q} = \mathcal{L}^{-1}(\Delta\xi) \quad (5)$$

such that the kinetic and potential energy coupling (near the reference structure) is reduced. Hence, similarly to the rectilinear normal coordinates, the linear combination coefficients can be obtained using the  $\mathbf{GF}$  method:

$$\mathcal{L}^{-1}\mathbf{GF}\mathcal{L} = \mathbf{\Lambda} \quad (6)$$

and the eigenvectors, in  $\mathcal{L}$ , of the  $\mathbf{GF}$  matrix provide us the linear combination coefficients of the c-normal coordinates.  $\mathbf{F}$  is the Hessian matrix of the PES

$$F_{ij} = \left( \frac{\partial^2 V}{\partial \xi_i \partial \xi_j} \right)_{\text{eq}} \quad (7)$$

computed with respect to the  $\xi_i$  curvilinear coordinates at the equilibrium (eq) structure. The matrix  $\mathbf{G}$  is obtained as

$$\mathbf{G} = \mathbf{B}\mathbf{M}^{-1}\mathbf{B}^T, \quad (8)$$

where  $\mathbf{M}$  is a  $3N \times 3N$  diagonal matrix containing the masses,  $m_a$  ( $a = 1, \dots, N$ ), of the atomic nuclei

$$\mathbf{M}^{-1} = \begin{pmatrix} 1/m_1 & & & 0 \\ & 1/m_1 & & \\ & & 1/m_1 & \\ & & & \ddots \\ 0 & & & & 1/m_N \end{pmatrix} \quad (9)$$

and  $\mathbf{B}$  is a  $\bar{D} \times 3N$  matrix that contains the derivatives of the internal coordinates with respect to the rectilinear displacements  $(\partial \xi_i / \partial d_{j\alpha})_{\text{eq}}$  ( $i = 1, \dots, \bar{D}$ ,  $j = 1, \dots, N$ ,  $\alpha = x, y, z$ ) and satisfy the following relation:

$$\begin{pmatrix} \xi_1 \\ \xi_2 \\ \vdots \\ \xi_{\bar{D}} \end{pmatrix} = \mathbf{B} \begin{pmatrix} d_{1x} \\ d_{1y} \\ d_{1z} \\ \vdots \\ d_{Nz} \end{pmatrix}. \quad (10)$$

To have a good description of the *cis-trans* torsional motion, we exclude the  $\tau$  torsional degree of freedom from the  $\mathbf{GF}$  calculation and the c-normal coordinates are defined for the remaining  $\bar{D} = 8$  (displacement) internal coordinates that exhibit small(er) amplitude motions.

For a given value of the  $\mathcal{Q}_k$  c-normal coordinates, the value of the  $\xi_i$  internal coordinates can be calculated using the eigenvectors in  $\mathcal{L}$  and the  $\xi_i^{(\text{eq})}$  equilibrium values:

$$\xi_i = \xi_i^{(\text{eq})} + \sum_{k=1}^{\bar{D}} \mathcal{L}_{i,k}^{(\text{eq})} \mathcal{Q}_k, \quad k = 1, \dots, \bar{D} (= 8) \quad (11)$$

Since HCOOH has two equilibrium configurations, we have two parameter sets:  $\{\boldsymbol{\xi}^{(\text{c})}, \mathcal{L}^{(\text{c})}\}$  and  $\{\boldsymbol{\xi}^{(\text{t})}, \mathcal{L}^{(\text{t})}\}$  (the parameters are deposited in the SOM).

#### D. Relaxed curvilinear normal coordinates along the torsional motion

Since we are interested in the overall vibrational dynamics of HCOOH, we cannot restrict the description to the *cis* or the *trans* well. Hence, we repeated the c-normal mode computation (with  $\bar{D} = 8$  degrees of freedom) along the large-amplitude motion at several points (*vide infra*) over the entire range of  $\tau \in [0, 2\pi)$ . During this computation, we relaxed the molecular structure along  $\tau$  by minimizing the potential energy (Fig. 4). The relaxed values of the internal coordinates that correspond to the minimal potential energy as a function of  $\tau$  are shown in Fig. 5. These

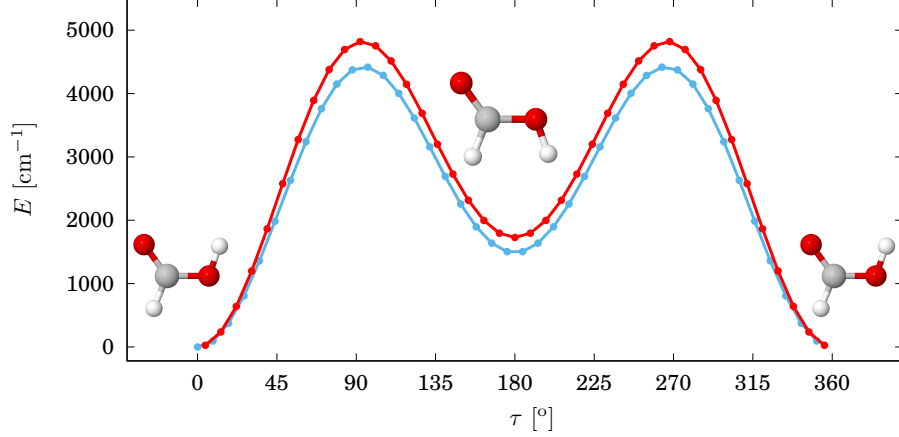


FIG. 4. 1-dimensional cut of the PES along the  $\tau$  torsional coordinate with (a) the non-torsional coordinates fixed at their equilibrium value at the global minimum (red); (b) relaxed non-torsional coordinates minimizing the potential energy (blue).

relaxed internal coordinate structures are considered as the ‘equilibrium structure’,  $\xi^{(\text{eq})}(\tau)$ , for the 8-dimensional c-normal-mode computation that is repeated for several  $\tau$  values.

In practice, the c-normal coordinates are computed (similarly to Sec. II C) at 24 equally distributed values of  $\tau = t_n$  with  $t_n = (n - 1)360^\circ/24$ ,

$$\xi_i(\tau) = \xi_i^{(\text{eq})}(\tau) + \sum_{j=1}^8 \tilde{\mathcal{L}}_{i,j}(\tau) \tilde{\mathcal{Q}}_j, \quad i = 1, \dots, 8. \quad (12)$$

Using the value of the coefficients at the  $t_n$  ( $n = 1, \dots, 24$ ) points, we interpolate  $\tilde{\mathcal{L}}_{i,j}(\tau)$  by solving a system of linear equations,

$$\tilde{\mathcal{L}}_{i,j}(t_n) = \sum_{k=1}^{24} c_k^{ij} f_k(t_n), \quad n = 1, \dots, 24. \quad (13)$$

For the  $f_k$  functions, we have considered the following functions of the Fourier basis

$$1, \cos(\tau), \sin(\tau), \cos(2\tau), \sin(2\tau), \dots, \cos(12\tau). \quad (14)$$

All coordinates can be expanded using only cosine functions of  $\tau$ , except for the  $\varphi$  out-of-plane bending (that is also a torsion-like, but small-amplitude vibration).  $\varphi$  is an odd function of  $\tau$  (Fig. 5), and hence sine basis functions are used for its interpolation.

As a result, we have relaxed equilibrium internal coordinates,  $\xi^{(\text{eq})}(\tau)$  and relaxed c-normal (rc-normal) mode  $\tilde{\mathcal{L}}_{i,j}(\tau)$  coefficients as a function of  $\tau$  (Figs. 5 and 6). The rc-normal coordinates incorporate in the coordinate definition the optimal structural changes along the  $\tau$  large-amplitude motion, while the kinetic and potential energy coupling is minimized among the small amplitude (normal) coordinates. This construct is expected to provide an almost ideal coordinate representation for this system. Results of convergence tests are reported in Sec. VI.

### III. QUANTUM HAMILTONIAN

The (ro)vibrational kinetic energy operator (KEO) corresponding to the torsional-relaxed-curvilinear-normal coordinate representation  $\mathbf{q} = (\tilde{\mathbf{Q}}, \tau)$  is constructed using the numerical KEO approach as implemented in the GENIUSH computer program [2]. The core of the program is based on the

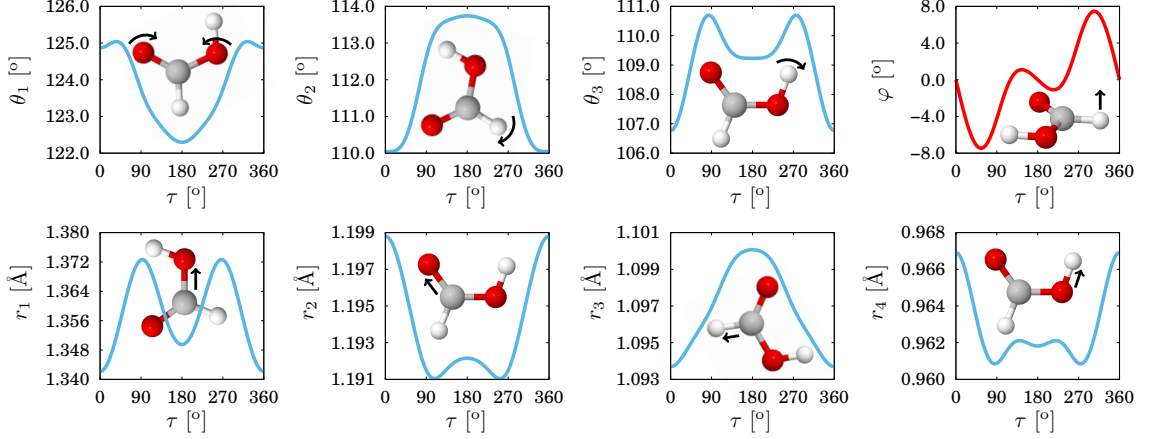


FIG. 5. Minimized equilibrium values for the internal coordinates as a function of the  $\tau$  torsional angle. The relaxed bond length and bond angle functions are symmetric with respect to  $\tau = 180^\circ$  (blue). The relaxed out-of-plane bending angle,  $\varphi$ , is anti-symmetric with respect to  $\tau = 180^\circ$  (red).

evaluation of the mass-weighted metric tensor at coordinate points:

$$g_{kl} = \sum_{i=1}^N m_i \mathbf{t}_{ik}^T \mathbf{t}_{il}; \quad k, l = 1, 2, \dots, 3N - 3 \quad (15)$$

where the so-called vibrational and rotational t-vectors are

$$\mathbf{t}_{ik} = \frac{\partial \mathbf{r}_i}{\partial q_k}; \quad k = 1, 2, \dots, 3N - 6 \quad (16)$$

$$\mathbf{t}_{i,3N-6+a} = \mathbf{e}_a \times \mathbf{r}_i; \quad a = 1(x), 2(y), 3(z), \quad (17)$$

respectively. For the computation of the t-vectors, and using them to construct the  $\mathbf{g} \in \mathbb{R}^{(3N-3) \times (3N-3)}$  matrix, it is necessary to know the body-fixed Cartesian coordinates  $\mathbf{r}_i$  ( $i = 1, \dots, N$ ) as a function of the generalized vibrational coordinates  $q_k$  ( $k = 1, \dots, 3N - 6$ ). We expect that an efficient representation can be obtained with the relaxed-curvilinear-normal coordinate plus torsion choice (Sec. II)

$$q_i = \tilde{Q}_i, \quad i = 1, \dots, 8 \\ q_{3N-6} = \tau. \quad (18)$$

The corresponding  $\mathbf{r}_i$  vs.  $q_k$  relations can be obtained from Eqs. (1) and (12). This coordinate choice results in an arrow-like structure of the  $\mathbf{G}$  matrix (Fig. 7), *i.e.*, the coupling of the  $\tau$  large-amplitude motion and the  $\tilde{\mathbf{Q}}$  small-amplitude coordinates is not necessarily small (can be large), but the coupling among the small-amplitude  $\tilde{\mathbf{Q}}$  coordinates is small for all  $\tau$  values.

The derivatives of the  $\mathbf{r}_i$  Cartesian coordinates with respect the  $q_k$  generalized internal coordinates are obtained by using the two-sided finite difference formula. The  $\mathbf{G} \in \mathbb{R}^{(3N-3) \times (3N-3)}$  matrix is obtained by inversion of  $\mathbf{g} \in \mathbb{R}^{(3N-3) \times (3N-3)}$ :

$$\mathbf{G} = \mathbf{g}^{-1}. \quad (19)$$

In most applications of GENIUSH [2–4, 34–38], the discrete variable representation [39] was

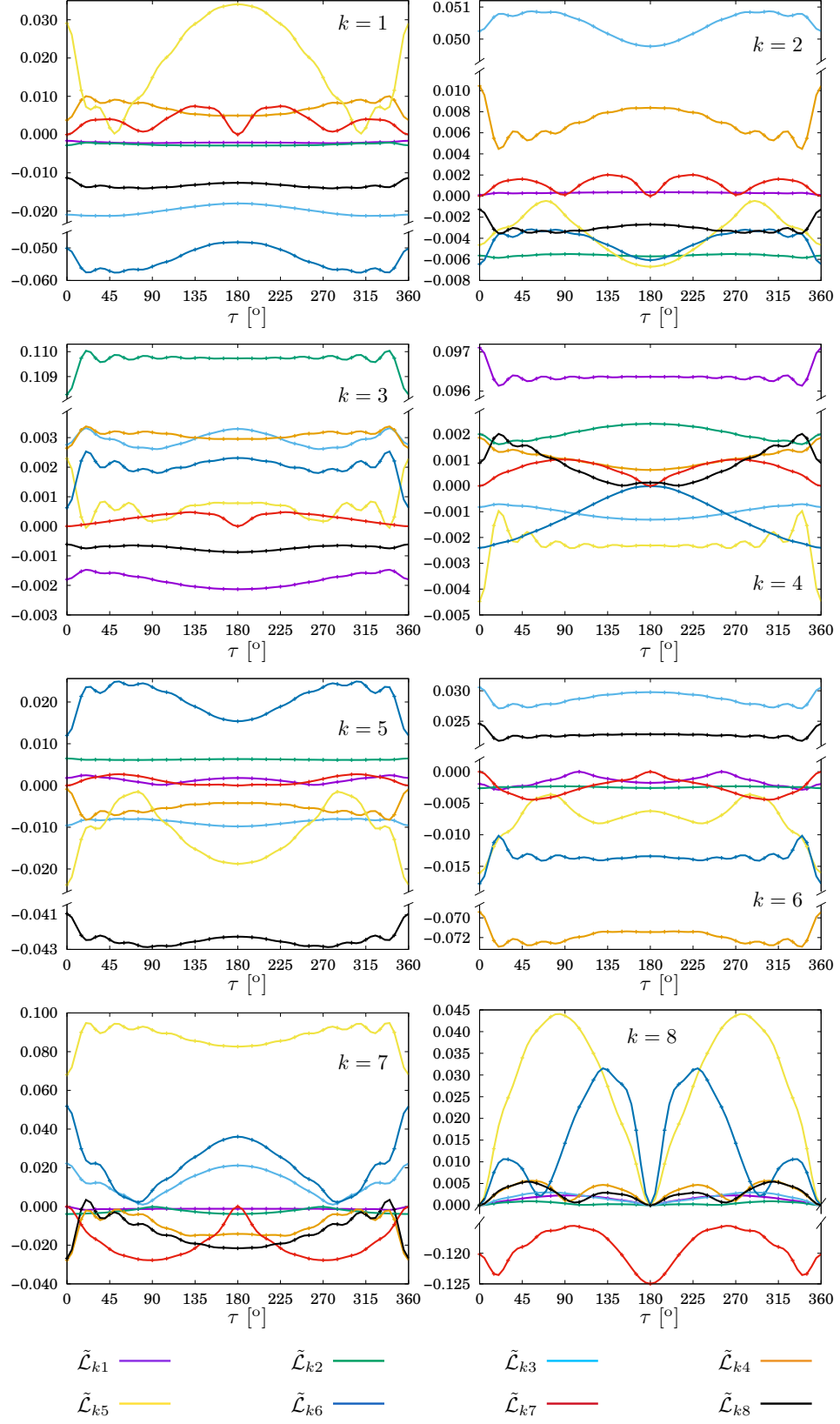


FIG. 6. Curvilinear normal coordinate coefficients, Eq. (12), as a function of the  $\tau$  torsional angle.



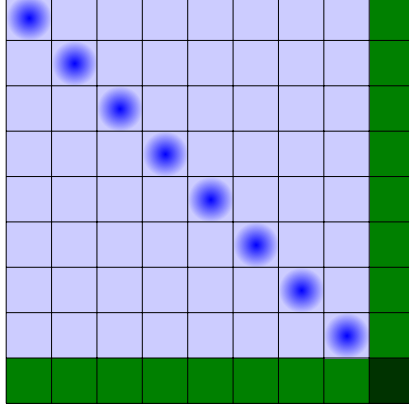


FIG. 7. Visualization of the  $\mathbf{G}$  matrix, Eqs. (15) and (19), for a (any) grid point from the dynamically relevant range. The eight rc-normal modes are weakly coupled among each other (light blue), but their weak coupling with the large amplitude motion ( $\tau$ ) is *not* assumed (dark green). The relaxation of the reference structure and the  $\mathbf{GF}$  diagonalization along  $\tau$  ensures that the coupling among the rc-normal coordinates remains small (light blue) for any value of  $\tau$  (see also Figs. 5 and 6).

used, and in that representation the Podolsky (P) form of the general vibrational KEO

$$\hat{H}^{\text{v,P}} = \frac{1}{2} \sum_{k=1}^D \sum_{l=1}^D \tilde{g}^{-1/4} \hat{p}_k G_{kl} \tilde{g}^{1/2} \hat{p}_l \tilde{g}^{-1/4} \quad \text{with} \quad \tilde{g} = \det \mathbf{g} \quad (20)$$

is an advantageous choice, because it requires only first-order coordinate derivatives.

In this work, we use a finite basis representation of the Hamiltonian (Secs. IV and V), and for this purpose the ‘fully rearranged’ form [16, 17, 40] is more convenient

$$\hat{H}^{\text{v}} = -\frac{1}{2} \sum_{i=1}^{3N-6} \sum_{j=1}^{3N-6} G_{ij} \frac{\partial}{\partial q_i} \frac{\partial}{\partial q_j} - \frac{1}{2} \sum_{i=1}^{3N-6} B_i \frac{\partial}{\partial q_i} + U + V \quad (21)$$

where  $G_{ij}$ ,  $B_i$ ,  $U$ , and  $V$  are functions of the vibrational coordinates,

$$B_i = \sum_{k=1}^{3N-6} \frac{\partial}{\partial q_k} G_{ki} \quad (22)$$

and the pseudo-potential term is

$$U = \frac{1}{32} \sum_{kl=1}^{3N-6} \left[ \frac{G_{kl}}{\tilde{g}^2} \frac{\partial \tilde{g}}{\partial \xi_k} \frac{\partial \tilde{g}}{\partial \xi_l} + 4 \frac{\partial}{\partial \xi_k} \left( \frac{G_{kl}}{\tilde{g}} \frac{\partial \tilde{g}}{\partial \xi_l} \right) \right]. \quad (23)$$

#### IV. BASIS FUNCTIONS AND TRUNCATION OF THE DIRECT-PRODUCT BASIS

We start expanding the wave function over a direct product of basis functions of the selected coordinates

$$\Psi_i(q_1, \dots, q_8, \tau) = \sum_{n_{q_1}=0}^b \dots \sum_{n_{q_8}=0}^b \sum_{n_\tau=0}^{N_\tau^{\max}} C_{n_{q_1}, \dots, n_{q_8}, n_\tau}^i \prod_{i=1}^8 \psi_{n_{q_i}}^{(i)}(q_i) \psi_{n_\tau}^{(\tau)}(\tau). \quad (24)$$

In this work, we use harmonic oscillator basis functions, for the (dimensionless)  $q_1, \dots, q_8$  rc-normal coordinates,

$$\psi_n(q) = A_n H_n(q) e^{-q^2/2} \quad \text{with} \quad q \in (-\infty, +\infty), \quad (25)$$

where  $H_n(q)$  is the  $n$ th-order Hermite polynomial and  $A_n$  is a normalization constant. Sec. V 1 provides further important technical details regarding the range of the different coordinate choices. Regarding the  $\tau$  torsional coordinate, we use a Fourier basis including the following functions,

$$1, \cos(\tau), \sin(\tau), \dots, \cos(n_\tau \tau), \sin(n_\tau \tau), \quad \tau \in [0, 2\pi) \quad (26)$$

to solve the 1-dimensional (1D) torsional Schrödinger equation,

$$\hat{H} = G_{\tau\tau} \frac{\partial^2}{\partial \tau^2} + \frac{\partial G_{\tau\tau}}{\partial \tau} \frac{\partial}{\partial \tau} + V_\tau, \quad (27)$$

where the pseudo-potential term, Eq. (23), is neglected. As a result, we obtain torsional functions that can be identified as *trans*, *cis*, or *delocalized* torsional functions explained and discussed in detail in Sec. VI. We use this 1D torsional basis set to solve the 9D vibrational problem of formic acid.

An accurate product basis set representation for the lowest vibrational levels of HCOOH requires values of  $N_\tau^{\max} > 30$  and  $b \geq 8$ . The number of functions in a direct product basis with  $N_\tau^{\max} = 30$  and  $b = 8$  is  $9^8 \cdot 31 \approx 1.3 \cdot 10^9$  that is too large for practical computations, and still not sufficient for good convergence. Since the couplings of the eight (relaxed) curvilinear normal coordinates was made small over the entire range of  $\tau$  (Sec. II), we may expect that the basis set can be efficiently pruned according to

$$\Psi_i = \sum_{n_\tau=0}^{N_\tau^{\max}} \sum_{f(n_{q_1}, \dots, n_{q_8}) \leq b} C_{n_{q_1}, \dots, n_{q_8}, n_\tau}^i \prod_{i=1}^8 \psi_{n_{q_i}}^{(i)}(q_i) \psi_{n_\tau}^{(\tau)}(\tau) \quad (28)$$

$$\text{with} \quad f(n_{q_1}, \dots, n_{q_8}) = n_{q_1} + \dots + n_{q_8}, \quad (29)$$

where certain basis functions have been discarded from the direct product. Eq. (29) gives the simplest possible pruning function. Poirier and co-workers [25–27] have studied more elaborate pruning conditions targeting very highly excited states.

Since the  $\psi_{n_{q_1}}(q_1) \dots \psi_{n_{q_8}}(q_8)$  product function provides a good representation for the small-amplitude (non- $\tau$ ) dynamics, we can discard basis functions based on simple physical arguments. For an *a priori* assessment about the importance of a basis function  $|\mathbf{n}'\rangle$  ( $\mathbf{n}'$  collects the basis indexes) in a wave function dominated by the  $|\mathbf{n}\rangle$  basis state, the smallness of the ratio of the Hamiltonian matrix element with respect to the difference of the zeroth-order energies,

$$\frac{\langle n_1, \dots, n_8, n_\tau | \hat{H} | n'_1, \dots, n'_8, n'_\tau \rangle}{E_{n_1, \dots, n_8, n_\tau}^{(0)} - E_{n'_1, \dots, n'_8, n'_\tau}^{(0)}} \approx 0 \quad (30)$$

can provide a good indication about the unimportance of  $|\mathbf{n}'\rangle$  for the variational result. The ratio is small, if (a) the Hamiltonian matrix element is small, and/or (b) the zeroth-order energy difference is large. The order of magnitude of the Hamiltonian matrix element can be estimated by considering the fast convergence of the Taylor expansion of the potential and the kinetic energy in rc-normal coordinates.

If the zeroth-order energy for a multi-dimensional basis function is very large, then the contribution of the function to the lowest-energy wave functions is negligible. For example, in order to compute the ground vibrational wave function, the 8D basis functions

$$\mathbf{0} = (0, 0, 0, 0, 0, 0, 0, 0) \quad \text{and} \quad 1_1, 2_1, 3_1, 4_1, 5_1, 6_1, 7_1, 8_1 \quad (31)$$

are necessary, since  $\langle \mathbf{0}, n_\tau | \hat{H} | n'_{q_1}, \dots, n'_{q_8}, n'_\tau \rangle$  is not small. In Eq. (31), we have introduced a short notation, we list only the degrees of freedom for which the basis function index (‘vibrational

quantum number') is larger than 0, *e.g.*,  $3_1 = (0, 0, 1, 0, 0, 0, 0, 0)$ .

Furthermore, less important, but still significant contribution to the ground vibrational state may be expected from the following 8D basis functions:

$$\begin{aligned}
 &1_2, 2_2, 3_2, 4_2, 5_2, 6_2, 7_2, 8_2, \\
 &1_1 2_1, 1_1 3_1, 1_1 4_1, 1_1 5_1, 1_1 6_1, 1_1 7_1, 1_1 8_1, \\
 &2_1 3_1, 2_1 4_1, 2_1 5_1, 2_1 6_1, 2_1 7_1, 2_1 8_1, \\
 &3_1 4_1, 3_1 5_1, 3_1 6_1, 3_1 7_1, 3_1 8_1, \\
 &4_1 5_1, 4_1 6_1, 4_1 7_1, 4_1 8_1, \\
 &5_1 6_1, 5_1 7_1, 5_1 8_1, \\
 &6_1 7_1, 6_1 8_1, \\
 &7_1 8_1,
 \end{aligned} \tag{32}$$

where we note that the functions with  $8_1$  contribution can be discarded for the present system (HCOOH) due to symmetry reasons. At the same time, the basis function  $1_1 2_1 3_1 4_1 5_1 6_1 7_1 8_1$  gives a negligible contribution to the lowest-energy states in comparison with the basis functions listed in Eqs. (31) and (32), since both the Hamiltonian matrix elements are expected to be small and the zeroth-order energy differences are large.

These kinds of arguments do not apply for discarding torsional functions, since the coupling of the  $\tau$  coordinate and the curvilinear normal modes (the Hamiltonian matrix element) may be large and the zeroth-order torsional energies are small, *i.e.*, both (a)–(b) pruning ‘criteria’ below Eq. (30) fail. Therefore, we retain all torsional basis functions in the basis set.

All in all, using the simplest pruning function in Eq. (29), the direct-product basis, Eq. (24), including  $1.3 \cdot 10^9$  functions can be reduced to  $4 \cdot 10^5$  functions, while the lowest (few hundred) vibrational states can be computed accurately.

For future work, we consider more elaborate pruning conditions. Based solely on the harmonic frequencies, the following condition could be formulated,

$$0 \leq 2n_{q_1} + 2n_{q_2} + \frac{3}{2}n_{q_3} + n_{q_4} + n_{q_5} + n_{q_6} + \frac{1}{2}n_{q_7} + n_{q_8} \leq b. \tag{33}$$

This condition accounts only for the denominator of Eq. (30). Since the higher-frequency harmonic oscillator modes correspond to the stretching degrees of freedom, the coupling through the Hamiltonian matrix element, numerator of Eq. (30), may be large. A ‘safe’ improvement of Eq. (29), reads as

$$0 \leq n_{q_1} + n_{q_2} + n_{q_3} + n_{q_4} + n_{q_5} + n_{q_6} + \frac{1}{2}n_{q_7} + n_{q_8} \leq b \tag{34}$$

that corresponds to increasing the number of basis functions for the lowest-frequency (totally symmetric) harmonic mode (O–C–O bending). We plan to use Eq. (34) in future work (see also Sec. VI).

## V. MULTI-DIMENSIONAL INTEGRATION

### 1. Coordinate ranges for curvilinear normal coordinates

Since we use harmonic oscillator basis functions, Eq. (25), it will be appropriate to use a set of (nested) Hermite quadratures to evaluate integrals for the matrix elements. Before doing that we need to address the question of the coordinate range for rc-normal coordinates.

The range of the harmonic oscillator functions and also of the Hermite quadrature is  $(-\infty, \infty)$ , whereas the range of the internal coordinates is more restricted:  $[0, \infty)$  for a stretching and  $[0, \pi]$  for a bending. At the same time, if we calculate the value of the curvilinear coordinates,  $\xi_i$ , using the values of rc-normal coordinates,  $\tilde{Q}_k$  (at grid points) according to Eq. (12), it can happen that we obtain a value that is outside the coordinate range (*e.g.*, negative value for a distance). Fortunately, this does not happen for grid points near the origin, but at the edges of the multi-

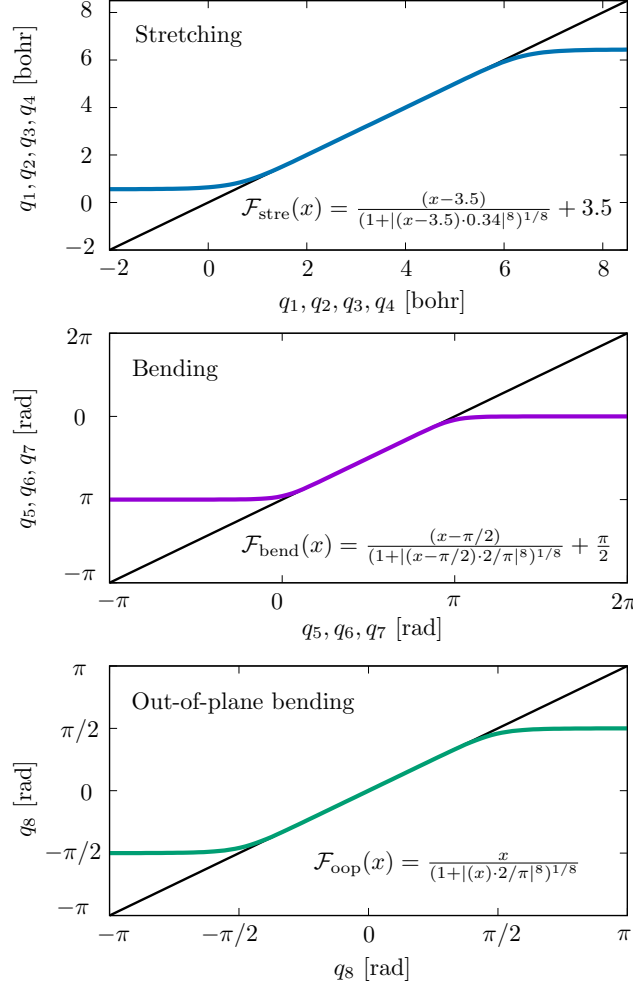


FIG. 8. Functions used for the stretching, bending, and out-of-plane bending coordinates to map the  $(-\infty, +\infty)$  range of the curvilinear normal coordinates to the mathematically appropriate and dynamically relevant range of HCOOH.

dimensional grid, there are points that return internal coordinate values outside their range. For rectilinear normal coordinates, this does not happen, since the body-fixed Cartesian coordinates are also defined over  $(-\infty, +\infty)$ .

To handle the problematic points of the rc-normal coordinate grid, we define mapping functions which ensure that the result is in the good range:

$$\mathcal{F} \left[ \xi_i^{(\text{eq})} + \sum_{k=1}^D \tilde{\mathcal{L}}_{ik} \tilde{Q}_k \right] \in \text{Range}(\xi_i). \quad (35)$$

Furthermore, we expect that a good mapping function behaves as a linear (an almost trivial) mapping within the good range, but it ensures that at the ‘edges’ of the multi-dimensional grid meaningful values are returned.

For a sigmoid-like mapping function,  $x \mapsto \arctan(x)$  and  $x \mapsto \tanh(x)$  are the most common examples. Unfortunately, outside the  $[-0.5, 0.5]$  interval, these functions significantly deviate from  $x \mapsto x$ , and we would like to find a function that is close to  $x \mapsto x$  over almost the entire coordinate range, but ensures that the ‘edges’ also have meaningful values. For these reasons, we decided to

use

$$\mathcal{F}(x) = \frac{x}{(1 + |x|^k)^{1/k}} \quad (36)$$

with  $k = 8$ . The procedure is simple. For a quadrature point  $\tau^{k_\tau}$  and  $q_1^{k_1}, \dots, q_8^{k_8}$ , the internal coordinates of the reference structure and the corresponding displacements are calculated. Their sum provides the ‘raw’ internal coordinate value that is mapped to the final value of the coordinate within the correct range. The following parameterization is used for the stretching ( $r_i$ ), bending ( $\theta_i$ ), and out-of-plane bending (oop,  $\varphi$ ) types of coordinates (Fig. 8)

$$\mathcal{F}_{\text{stre}}(x) = \frac{(x - 3.5)}{(1 + |(x - 3.5) \cdot 0.34|^8)^{1/8}} + 3.5, \quad (37)$$

$$\mathcal{F}_{\text{bend}}(x) = \frac{(x - \pi/2)}{(1 + |(x - \pi/2) \cdot 2/\pi|^8)^{1/8}} + \frac{\pi}{2}, \quad (38)$$

and

$$\mathcal{F}_{\text{oop}}(x) = \frac{x}{(1 + |(x) \cdot 2/\pi|^8)^{1/8}}, \quad (39)$$

respectively. These functions ensure that the ‘final’ value for the stretching coordinates is within the  $[0.56, 6.44]$  bohr interval, which is the relevant dynamical range for all stretches in HCOOH, the value of the bending coordinate is within  $[0, \pi]$ , and the out-of-plane bending is within  $[-\pi/2, \pi/2]$ . Although  $\varphi$  is a torsion-like coordinate and is defined on  $[-\pi, \pi]$ , it is a small(er) amplitude vibration of formic acid, and the relevant dynamical range is within  $[-\pi/2, \pi/2]$ .

Regarding Eq. (36), we decided to use  $k = 8$  because it appears to be a good compromise between a faithful mapping (of the good range) and numerical integrability of the matrix elements with a reasonable number of points. Nevertheless, we have checked values up to  $k = 14$  using a pruned basis set with  $b = 8$  (Sec. IV), and we obtained the vibrational energies within  $0.03 \text{ cm}^{-1}$  from the  $k = 8$  values (using the same basis) up to  $3000 \text{ cm}^{-1}$  beyond the zero-point energy.

### A. Smolyak quadrature

We use the Smolyak approach [6, 13–15, 18, 41] to construct efficient non-product grids for the pruned basis set, Eqs. (28)–(29), that can be used to evaluate the multi-dimensional integrals appearing in the kinetic energy coefficients, Eq. (21), and in the PES. The Smolyak quadrature for nine dimensions is defined as

$$Q(9, H) = \sum_{\sigma_s(i) \leq H} \otimes \prod_{\chi=1}^9 \Delta \hat{Q}_\chi^{i_{q_\chi}}, \quad i_\chi = 1, 2, 3, 4, \dots, \chi = 1, \dots, 9$$

with  $\sigma_s(i) = s^\tau(i_\tau) + s^{q_1}(i_{q_1}) + \dots + s^{q_8}(i_{q_8})$ , (40)

where  $H$  is a grid-pruning parameter,  $\sigma_s(i)$  is a grid-pruning function, and the incremental operator is defined as

$$\Delta \hat{Q}_\chi^{i_\chi} = \hat{Q}_\chi^{i_\chi} - \hat{Q}_\chi^{i_\chi - 1} \quad (41)$$

with  $\hat{Q}_\chi^0 = 0$  and the 1D quadrature rules,

$$\hat{Q}_\chi^{i_\chi} f(q_\chi) = \sum_{m=1}^{m_{i_\chi}} w_{\chi, m}^{i_\chi} f(q_{\chi, m}^{i_\chi}), \quad i_\chi = 1, 2, 3, 4, \dots \quad (42)$$

Equivalently, we can also write the Smolyak quadrature as a linear combination of product quadratures with different 1-dimensional accuracies as

$$Q(9, H) = \sum_{\sigma_s(i) \leq H} C_i \left( \otimes \prod_{\chi=1}^9 \hat{Q}_{i_\chi}^{i_\chi} \right), \quad i_\chi = 1, 2, 3, 4, \dots, \chi = 1, \dots, 9, \quad (43)$$

$$\text{with } \sigma_s(i) = s^\tau(i_\tau) + s^{q_1}(i_{q_1}) + \dots + s^{q_8}(i_{q_8}). \quad (44)$$

$Q(9, H)$  has a smaller number of points, than the direct product grid,  $\hat{Q}_{q_1}^{i_{q_1}^{\max}} \otimes \dots \otimes \hat{Q}_{q_8}^{i_{q_8}^{\max}} \otimes \hat{Q}_\tau^{i_\tau^{\max}}$ , and its accuracy depends on three factors, (a) the form of the  $s^\chi(i_\chi)$  grid pruning functions, for which  $s^\chi(i_\chi) \geq s^\chi(i_\chi - 1)$  must hold; (b) the grid-pruning parameter  $H$ ; and (c) the number of the  $m_{i_\chi}$  grid points, for which  $m_{i_\chi} \geq m_{i_\chi - 1}$  must hold.

For constructing the Smolyak grid in the present work, we define the  $s^\chi(i_\chi)$  functions as follows:

$$\chi = \tau : \quad s^\chi(i_\chi) = 10 \quad (45)$$

$$\chi = q_1, \dots, q_8 : \quad s^\chi(i_\chi) = 10i_\chi, \quad i_\chi = 1, 2, 3, \dots \quad (46)$$

The value of  $H$ , which sets an upper limit on the sum of the  $s$  function values, is chosen according to this definition. The sequences of quadrature rules  $\hat{Q}_\chi^{i_\chi}$  are chosen as

$$\begin{aligned} \chi = \tau : \quad \hat{Q}_\tau^{i_\tau} &= \hat{Q}_{M_\tau^{\max}}^{\text{trap}}, \quad i_\tau = 1, 2, 3, \dots \\ \chi = q_1, \dots, q_8 : \quad \hat{Q}_\chi^{i_\chi} &= \hat{Q}_{m_{i_\chi}}^{\text{Her}}, \quad i_\chi = 1, 2, 3, \dots \\ \text{with } m_{i_\chi} &= 1, 3, 3, 7, 9, 9, 9, 9, 17, 19, 19, 19, 31, 33, 41, 41, \dots \end{aligned} \quad (47)$$

where  $\hat{Q}_{M_\tau^{\max}}^{\text{trap}}$  is a trapezoidal quadrature rule of  $M_\tau^{\max}$  points and a maximum degree of  $d_\tau = 2M_\tau^{\max} - 1$ , while  $\hat{Q}_{m_{i_\chi}}^{\text{Her}}$  are nested quadrature rules for Hermite polynomials with a maximum degree of  $d_{i_\chi} = 1, 5, 5, 7, 15, 15, 15, 15, 17, 29, 29, 29, 31, 33, 61, 61, \dots$  corresponding to  $i_\chi = 1, 2, 3, \dots$  [42] Nesting means that all quadrature points of the quadrature rule  $\hat{Q}^j$  appear in the higher-order quadrature rule,  $\hat{Q}^{j+1}$ .

Using this construct with  $M_\tau = 11$  trapezoidal points and  $H = 150$ , we can integrate exactly all overlap matrix elements for the pruned basis set with  $0 \leq n_\tau \leq 4$  and  $0 \leq n_{q_1} + \dots + n_{q_8} \leq 8$  conditions. For  $H = 170$ , the Smolyak grid includes  $1\,230\,251 \approx 1.2 \cdot 10^6$  points. The smallest 9D direct-product Gauss grid that integrates correctly the same overlap matrix would have  $11 \cdot 9^8 \approx 4.7 \cdot 10^8$  points.

The Smolyak algorithm using nested sequences of quadrature rules allows us to use a non-product grid that has a structure, *i.e.*, a multi-dimensional integral of a function  $F(x_1, \dots, x_9)$  can be written as

$$\int F(x_1, \dots, x_9) dx_1 \dots dx_9 \approx \sum_{k_1=1}^{k_1^{\max}} \dots \sum_{k_9=1}^{k_9^{\max}} W^{\text{Smol}}(k_1, \dots, k_9) F(x_1^{k_1}, \dots, x_9^{k_9}), \quad (48)$$

where  $W^{\text{Smolyak}}(k_1, \dots, k_9)$  is the multi-dimensional Smolyak weight and the points are sorted according to the sequence of quadrature rules. The structure appears in the  $k_c^{\max}$  indexes.  $k_1$  depends on  $H$ ,  $k_2$  depends on  $H$  and  $k_1$ , etc. and thus, matrix-vector products can be computed by sequential summation [13, 15–17, 40, 43–45]. Eigenvalues and eigenvectors are computed using a Lanczos iterative eigensolver that requires only the multiplication of the Hamiltonian matrix with a vector. Implementation details regarding the matrix-vector multiplication has been described in Refs. [13, 15, 16].

## VI. NUMERICAL RESULTS

We have computed the vibrational energies using the basis set and pruning condition defined in Eqs. (28) and (29). The number of torsional basis functions was 55 and we used 79 grid points for this degree of freedom. Regarding the 8-dimensional (8D) rc-normal coordinate part of the

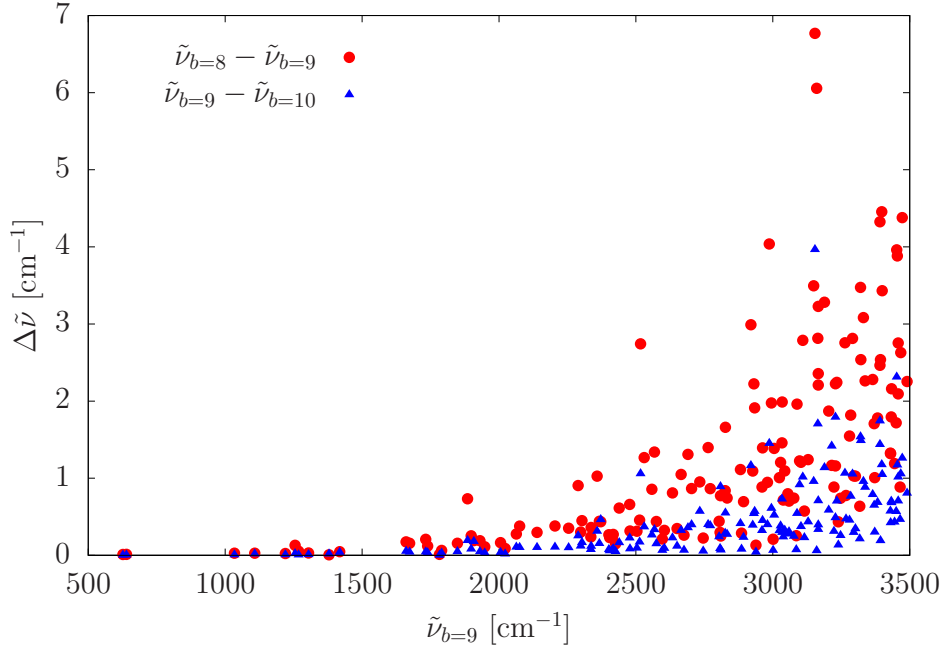


FIG. 9. Assessment of the convergence of the vibrational band origin obtained with a  $b = 9$  pruned basis set, Eqs. (28)–(29), using relaxed curvilinear (rc-) normal coordinates for the non-torsional degrees of freedom. The vibrational energies are compared with smaller ( $b = 8$ ) and larger ( $b = 10$ ) basis-set results. The zero-point energy with  $b = 8, 9$ , and  $10$  is  $\tilde{\nu}_0 = 7350.84, 7350.82$ , and  $7350.81 \text{ cm}^{-1}$ , respectively.

problem, three basis set sizes were used with the  $b = 8, 9$ , and  $10$  basis pruning parameter and with the  $H = 190, 200$ , and  $210$  grid pruning parameter, respectively. As a result, the 9D basis sets with  $b = 8, 9$ , and  $10$  included 707 850, 1 337 050, and 2 406 690 basis functions, respectively. The size of the corresponding non-product Smolyak quadrature grid was 42 223 623, 72 656 063 and 132 043 839.

The value of  $H$  was selected to be able to exactly integrate the Hamiltonian matrix elements up to 5th order (in a hypothetical Taylor expansion) with the highest-excited basis functions in the pruned basis set. Of course, we have checked the effect of using a larger  $H$  value. For  $H = 200$  (instead of  $H = 190$ ) with  $b = 8$ , the eigenvalues up to  $5000 \text{ cm}^{-1}$ , beyond the zero-point vibrational energy (ZPVE), changed at most by  $0.001 \text{ cm}^{-1}$ . Based on these observations, we think that the procedure is almost perfectly variational, which corresponds to an exact integration and provides rigorous energy upper bounds. Further computations with the more elaborate pruning condition in Eq. (34), with larger basis and grid sizes are in progress and will allow us to have access to well-converged vibrational energies beyond  $2000 \text{ cm}^{-1}$  above the ZPVE.

Convergence properties have been tested with respect to the basis set size (Fig. 9) and the coordinate representation (Fig. 10). Figure 9 shows that the vibrational energies with  $b = 9$  are converged better than  $1 \text{ cm}^{-1}$  up to ca.  $2500 \text{ cm}^{-1}$ , and within ca.  $2 \text{ cm}^{-1}$  up to  $3500 \text{ cm}^{-1}$  beyond the ZPVE.

Figure 10 highlights the efficiency of the rc-normal coordinates (Sec. II) in comparison with the rectilinear normal coordinates (for the non-torsional degrees of freedom). For the  $b = 8$  basis, the rectilinear normal coordinate vibrational energies differ (are less accurate) by  $8\text{--}10 \text{ cm}^{-1}$  from the rc-normal coordinate results.

We have also tested the coordinate definition of Lauvergnat and Nauts who computed the vibrational states of the methanol molecule in full dimensionality (12D) [6]. They did not relax and interpolate the normal coordinate coefficients along the large-amplitude coordinate, but they calculated the average of the (curvilinear) normal coordinate coefficients at the two local minima, hence we may call their coordinates averaged, curvilinear (ac-) normal coordinates. For HCOOH, we have performed computations both with ac- and rc-normal coordinates with the  $b = 8$  basis set. We have found that (for the present system) the relaxed curvilinear (rc-) normal coordinates slightly outperform simple averaging (ac-normal coordinates), but the difference is typically less

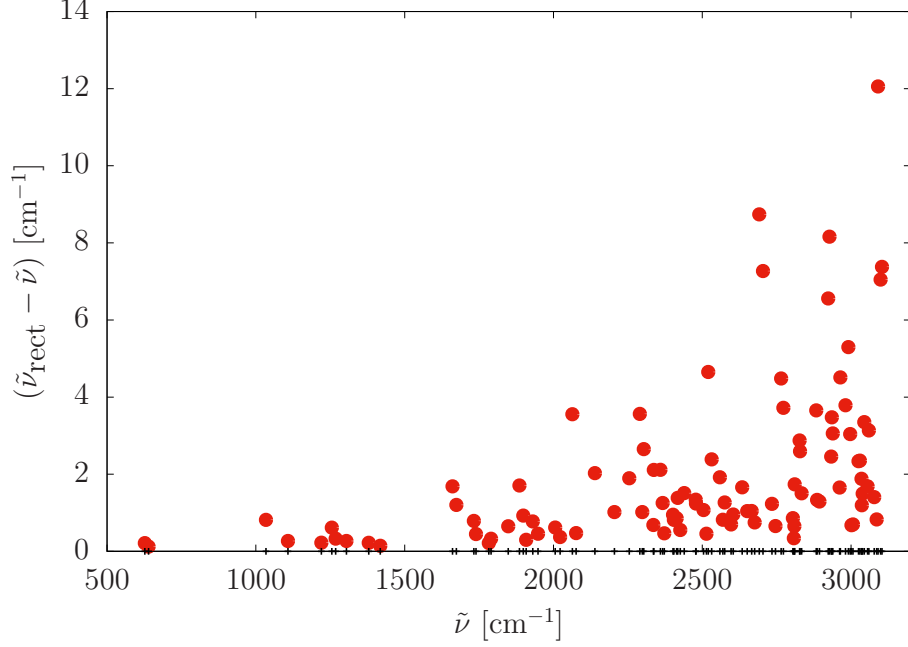


FIG. 10. Difference between the vibrational energies obtained using rectilinear,  $\tilde{\nu}_{\text{rect}}$ , and relaxed curvilinear (rc-),  $\tilde{\nu}$ , normal coordinates for the non-torsional degrees of freedom. In both cases the pruned basis set corresponds to the  $b = 8$  parameter, Eqs. (28)–(29). The corresponding ZPVEs are  $\tilde{\nu}_0 = 7350.84 \text{ cm}^{-1}$  and  $\tilde{\nu}_{\text{rect},0} = 7350.91 \text{ cm}^{-1}$ .

TABLE I. Plane reflection symmetry ( $C_s$  point group) with respect to the equilibrium structures of the one-dimensional basis functions used in the computations (Sec. IV). The first 22 1-dimensional (1D) torsional functions ( $c, t, d$ ) are plotted in Fig. 11. ( $n = 0, 1, 2, \dots, m = 1, 2, \dots$ )

A'	A''
$1_n, 2_n, 3_n, 4_n, 5_n, 6_n, 7_n$	–
$8_0, 8_2, \dots, 8_{2n}$	$8_1, 8_3, \dots, 8_{2n+1}$
$t_0, t_2, t_4, t_6$	$t_1, t_3, t_5, t_7$
$c_0, c_2, c_4, c_6$	$c_1, c_3, c_5$
$d_0, d_3, d_4, \dots, d_{4m-1}, d_{4m}$	$d_1, d_2, d_5, d_6, \dots, d_{4m-3}, d_{4m-2}$

than  $0.5 \text{ cm}^{-1}$  in the higher energy range. Hence, the ac-normal coordinates appear to be an excellent choice and they are technically much simpler to construct than the rc-normal coordinates used in the present work. Nevertheless, if there are multiple minima, stronger coupling of the large-amplitude motion with the ‘rest’ of the molecule, or more than one large-amplitude motions, then we can anticipate that the relaxation-interpolation approach used in the present work is, in principle, more efficient.

### A. Torsional assignment

Since the computation is not localized to one of the wells of the PES (Fig. 11), it is a relevant question to ask whether a given state can be assigned to the *trans* or the *cis* conformer. The torsional assignment of the 9D wave functions was performed based on the contribution of the 1D torsional basis functions (Fig. 11). Unless the torsional energy is very high, the torsional functions are localized in the *trans* or in the *cis* well, *i.e.*, they have a well-defined number of nodes beyond the ground state in ‘their’ well. The 1D torsional functions are eigenfunctions of the Schrödinger equation with the 1D torsional Hamiltonian, Eq. (27). There are eight 1D *trans* torsional functions ( $t_0, t_1, \dots, t_7$ ) and there are seven 1D *cis* torsional functions ( $c_0, c_1, \dots, c_6$ ). Beyond these states, the torsional functions have nodes in both wells and we call them *delocalized* functions. Each



torsional function has a well-defined parity with respect to reflection to the plane of the equilibrium structures (Table I). The torsional assignment of a 9D vibrational state was performed based on the assignment of the dominant torsional function. The plane reflection symmetry of the 9D vibrational wave function can be determined by the symmetry of the torsional functions and the symmetry of the out-of-plane vibrational mode (Table I).

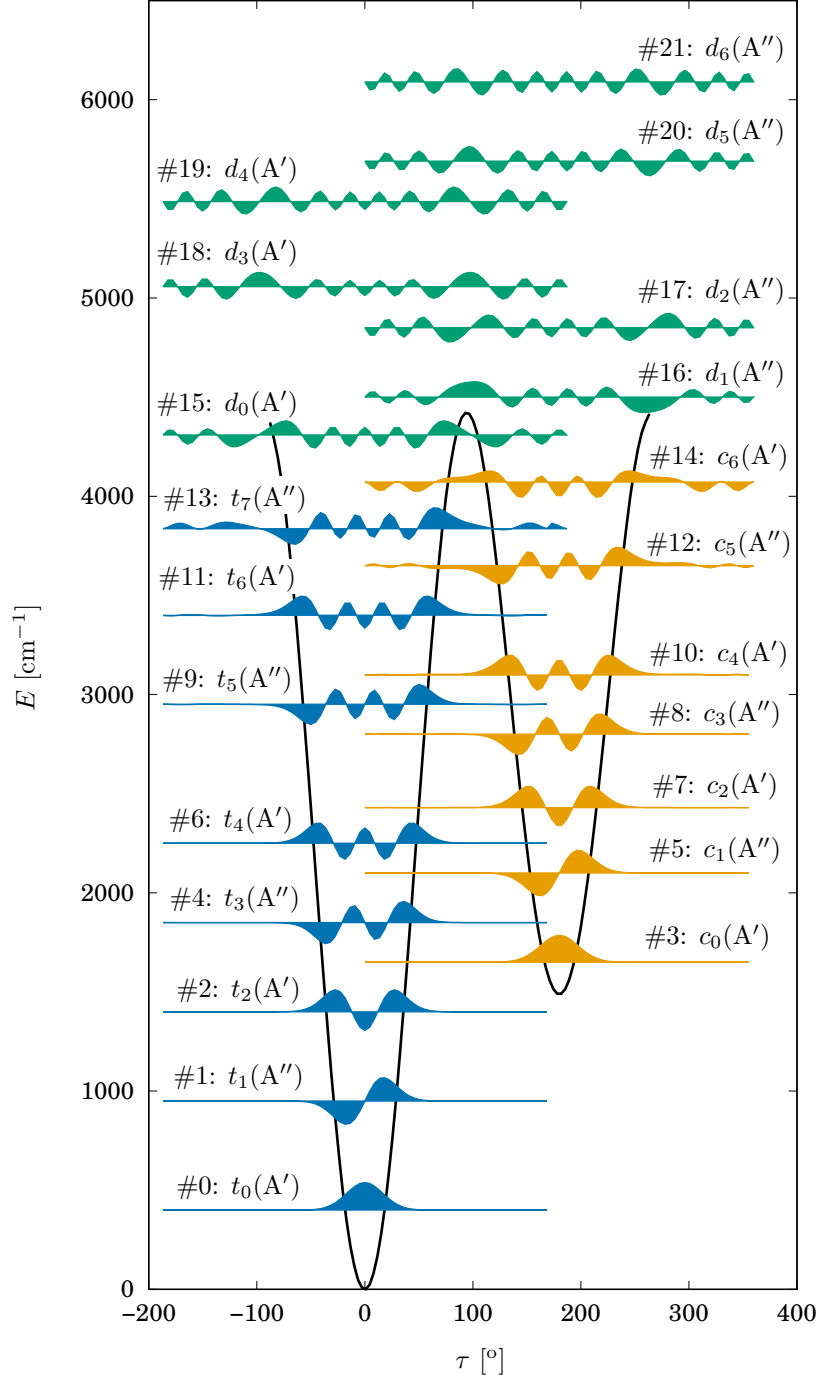


FIG. 11. Visualization of the *trans*- (blue), the *cis*- (yellow), and the lowest-energy *delocalized* (green) 1D torsional functions that were obtained by solving the 1D torsional Schrödinger equation, Eq. (27). The symmetry properties of the functions with respect to reflection to the plane defined by the equilibrium structures ( $\tau = 0^\circ$  and  $180^\circ$  in the figure) are collected in Table I.

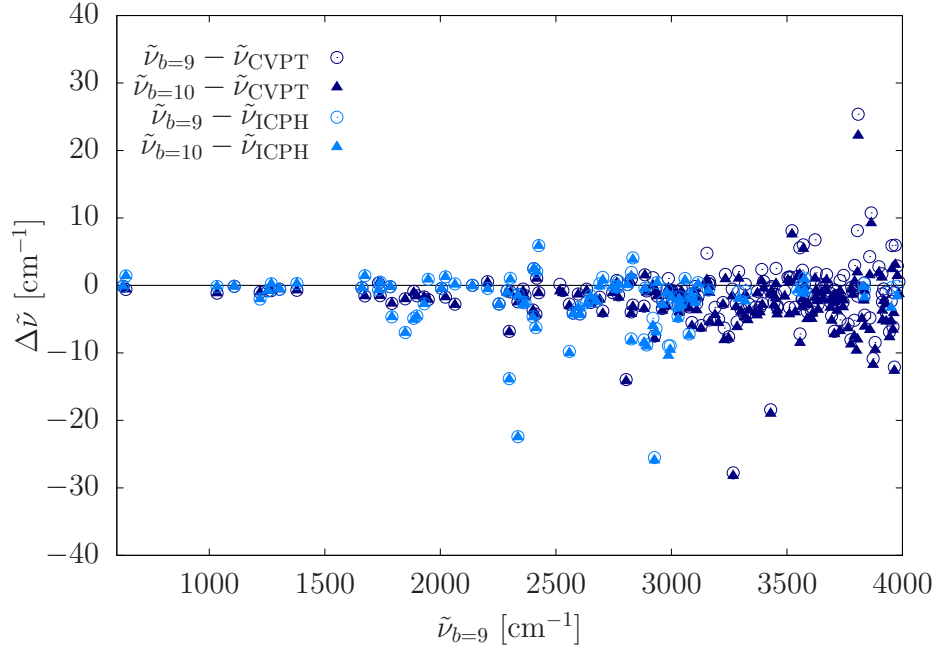


FIG. 12. Comparison of *trans*-HCOOH vibrational energies,  $\tilde{\nu}$  referenced to the zero-point energy, computed with the GENIUSH-Smolyak approach using the  $b = 9$  and  $10$  basis sets, Eqs. (28) and (29), and the 6th-order canonical van Vleck perturbation theory (CVPT) [30] and the internal-coordinate path Hamiltonian (ICPH) [28] results. The states from the different computations were compared based on the assignment of their wave function (Tables II–III). The zero-point energies are  $\tilde{\nu}_{\text{ZPV}} = 7351 \text{ cm}^{-1}$  ( $b = 9$  and  $10$ ) and  $\tilde{\nu}_{\text{ICPH,ZPV}} = 7354 \text{ cm}^{-1}$ .

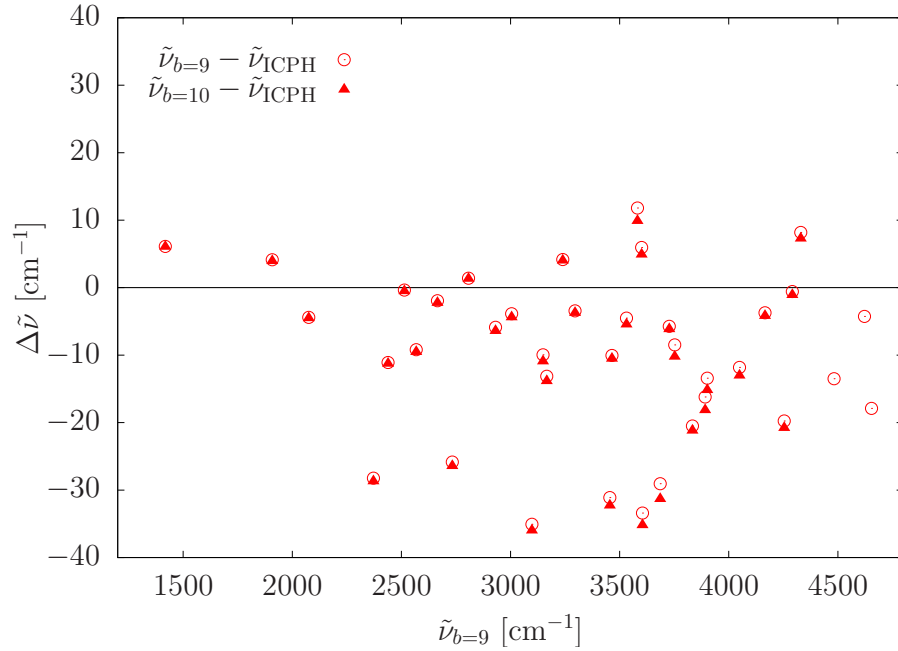


FIG. 13. Comparison of the *cis*-HCOOH vibrational energies,  $\tilde{\nu}$  referenced to the zero-point energy, computed with the GENIUSH-Smolyak approach using the  $b = 9$  and  $10$  basis sets, Eqs. (28) and (29), and the internal-coordinate path Hamiltonian (ICPH) [28] results. The states from the different computations were compared based on the assignment of their wave function (Tables IV and V). The (*trans*)-zero-point energies are  $\tilde{\nu}_{\text{ZPV}} = 7351 \text{ cm}^{-1}$  ( $b = 9$  and  $10$ ) and  $\tilde{\nu}_{\text{ICPH,ZPV}} = 7354 \text{ cm}^{-1}$ .

Regarding the *trans* states computed with the GENIUSH-Smolyak approach ( $b = 9$  and  $10$ ), we observe an overall good agreement with the internal-coordinate path Hamiltonian (ICPH) [28] and a very good agreement with the 6th-order canonical van Vleck perturbation theory (CVPT) [30] results (Fig. 12). The present variational computations systematically improve upon the CVPT results by 5–10(–25)  $\text{cm}^{-1}$  up to 4000  $\text{cm}^{-1}$  beyond the ZPVE. The good agreement of the *trans* vibrational energies (and assignments) with CVPT is interesting, since the CVPT computation was based on a single-well description and the *cis* zero-point vibration is only 1418  $\text{cm}^{-1}$  higher than the *trans* ZPVE, but it can be explained by the relatively high *cis-trans* isomerization barrier (Fig. 11).

The current (almost perfectly variational) computation improves the CVPT results by 1–5  $\text{cm}^{-1}$  in the range up to ca. 2500  $\text{cm}^{-1}$ , and by ca. 5–15  $\text{cm}^{-1}$  in the 2500–4000  $\text{cm}^{-1}$  range. We can spot one important outlier from this favorable comparison at around 3808  $\text{cm}^{-1}$  (Fig. 12). For this state the GENIUSH-Smolyak ( $b = 9$ ) energy is by 25  $\text{cm}^{-1}$  *higher* than the CVPT energy, and by comparing the  $b = 9$  and  $10$  energies, it is unlikely that some further enlargement of the basis set ( $b = 11, 12$ ) reduces this deviation to a value below 5  $\text{cm}^{-1}$ . This state is unambiguously assigned to  $7_6t_0$  in both computation, which is the 6th excitation of the lowest-energy, totally symmetric harmonic mode ( $\nu_7$ ). By considering the currently used pruning condition, Eq. (29), and the  $b = 8, 9, 10$  (11, 12) values of the pruning parameters (that are computationally feasible), we think that for this state our result is in an error and CVPT makes a (probably) good prediction. We can improve the GENIUSH-Smolyak results, without significantly increasing the computational cost, by using the more elaborate pruning condition in Eq. (34). The Eq. (34) pruning simply allows to double the number of basis functions for the totally symmetric, lowest-frequency mode, while keeping the size of the multi-dimensional basis within reasonable limits. Further work in this direction is in progress and will be reported in the future.

Regarding the *cis* states, the computed fundamentals agree well from all computations (GENIUSH-Smolyak, ICPH, and CVPT). We note that the highest energy  $c_1$  vibration is not (yet) available from the GENIUSH-Smolyak computations (this work), nor from ICPH Ref. [28]. Although CVPT results are available for all *cis* fundamental vibrations [30], combination and overtone bands have not been reported.

Figure 13 shows the comparison for *cis* states up to two excitations (based on the wave function assignments, Tables IV–V) of the GENIUSH-Smolyak ( $b = 9, 10$ ) and the ICPH [28] results. Similarly to the *trans* energies, there is an overall good agreement, but several ICPH energies are too high (by 10–40  $\text{cm}^{-1}$ ).

Beyond 3700  $\text{cm}^{-1}$  (above the *trans*-ZPVE), we can see mixed *cis-trans* states, in which torsional functions corresponding to the *trans* and other functions corresponding to the *cis* well are entangled (Tables IV–V). Several *cis-trans* entangled states come in pairs corresponding to + and – combinations of *cis* and *trans* basis functions. The corresponding ‘tunneling splittings’, which we currently compute to be  $< 1 - 5(-10)$   $\text{cm}^{-1}$ , are smaller or on the borderline with respect to the convergence uncertainty of the  $b = 9$  basis in the relevant energy range (indicated by  $(\delta_{10}, \delta_8)$  in the tables), and we plan to determine these splittings more precisely in future work.

Beyond 3900  $\text{cm}^{-1}$  (above the *trans*-ZPVE), non-negligible contribution from delocalized torsional states (Fig. 11) can be observed. Table VI shows the lowest-energy vibrational states with a significant delocalized contribution (see also Tables IV–V). These states have an energy close to the *cis-trans* isomerization barrier height (Fig. 11) and in this range the *cis-trans-delocalized* functions strongly mix and for their good description a variational procedure appears to be necessary. Further, better converged results will be reported in future work.

TABLE II. *Trans*-HCOOH: vibrational excitation energies,  $\tilde{\nu}$  in  $\text{cm}^{-1}$ , computed with the GENIUSH-Smolyak approach in comparison with the sixth-order canonical van Vleck perturbation theory (CVPT) [30] and the internal-coordinate reaction-path Hamiltonian (ICPH) [28] results. (The footnotes are below Table III.)

# <sup>a</sup>	Assign. <sup>b</sup>	$\tilde{\nu}$	$(\delta_{10}, \delta_8)^c$	CVPT	ICPH	# <sup>a</sup>	Assign. <sup>b</sup>	$\tilde{\nu}$	$(\delta_{10}, \delta_8)^c$	CVPT	ICPH
1	ZPV- $t_0$	7351	(0,0)	[n.a.]	7354	71	$6_2 7_1 t_0$	2827	(1,2)	2826	2825
2	$7_1 t_0$	627	(0,0)	627	627	72	$6_2 t_1$	2833	(0,1)	2836	2829
3	$t_1$	639	(0,0)	640	638	73	$7_1 8_1 t_2$	2882	(0,1)	2885	2890
4	$8_1 t_0$	1034	(0,0)	1035	1034	74	$3_1 6_1 t_0$	2886	(0,0)	2884	2886
5	$6_1 t_0$	1108	(0,0)	1108	1108	75	$6_1 t_3$	2893	(0,1)	2894	2902
6	$t_2$	1220	(0,0)	1221	1222	76	$7_3 8_1 t_0$	2920	(1,3)	2919	2925
7	$7_2 t_0$	1255	(0,0)	1256	1256	77	$[7_1 t_4, 6_1 7_1 t_2]$	2926	(0,1)	2934	2952
8	$7_1 t_1$	1268	(0,0)	1269	1268	79	$7_2 8_1 t_1$	2934	(1,2)	2934	2940
9	$5_1 t_0$	1304	(0,0)	1305	1305	80	$2_1 t_0$	2938	(0,0)	2940	2938
10	$4_1 t_0$	1379	(0,0)	1380	1379	81	$[7_1 t_4, 6_1 7_1 t_2]$	2961	(0,1)	2964	3066
12	$7_1 8_1 t_0$	1661	(0,0)	1661	1661	82	$5_1 7_1 8_1 t_0$	2963	(0,1)	2965	2965
13	$8_1 t_1$	1673	(0,0)	1675	1672	83	$5_1 8_1 t_1$	2980	(0,1)	2983	2981
14	$6_1 7_1 t_0$	1732	(0,0)	1732	1733	84	$6_1 7_3 t_0$	2987	(1,4)	2986	2996
15	$6_1 t_1$	1739	(0,0)	1741	1739	85	$6_1 7_2 t_1$	2995	(1,2)	2996	3004
16	$3_1 t_0$	1783	(0,0)	1783	1783	86	$3_1 t_2$	3001	(0,0)	3002	3003
17	$t_3$	1790	(0,0)	1793	1795	88	$3_1 7_2 t_0$	3024	(0,1)	3025	3027
18	$7_1 t_2$	1848	(0,0)	1850	1855	89	$[5_1 6_1 7_1 t_0]$	3028	(0,1)	3030	3033
19	$7_3 t_0$	1885	(0,1)	1886	1890	91	$[5_1 6_1 t_1]$	3034	(0,2)	3038	3036
20	$7_2 t_1$	1898	(0,0)	1900	1903	92	$3_1 7_1 t_1$	3038	(0,1)	3040	3041
22	$5_1 7_1 t_0$	1930	(0,0)	1932	1933	93	$4_1 7_1 8_1 t_0$	3043	(0,1)	3044	3046
23	$5_1 t_1$	1948	(0,0)	1950	1947	94	$[7_1 t_1, 7_2 t_3]$	3055	(0,1)	3057	[3109]
24	$4_1 7_1 t_0$	2006	(0,0)	2006	2006	95	$4_1 8_1 t_1$	3059	(0,1)	3061	3058
25	$4_1 t_1$	2022	(0,0)	2024	2021	96	$[5_1 t_3]$	3077	(0,1)	3080	3084
26	$8_2 t_0$	2063	(0,0)	2066	2063	97	$3_1 5_1 t_0$	3086	(0,0)	3087	3087
28	$6_1 8_1 t_0$	2139	(0,0)	2139	2139	98	$8_3 t_0$	3089	(1,2)	3094	3090
29	$6_2 t_0$	2205	(0,0)	2204	2205	100	$4_1 6_1 7_1 t_0$	3103	(0,1)	3103	3105
30	$8_1 t_2$	2254	(0,0)	2257	2257	101	$[7_3 t_2]$	3109	(1,3)	3112	[3144]
31	$7_2 8_1 t_0$	2289	(0,1)	2290	2290	102	$4_1 6_1 t_1$	3115	(0,1)	3117	3115
32	$[t_4, 6_1 t_2, 5_1 t_2]$	2298	(0,0)	2305	2312	103	$[5_2 7_1 t_0]$	3129	(0,1)	3135	[3159]
33	$7_1 8_1 t_1$	2303	(0,0)	2304	2302	105	$7_5 t_0$	3154	(4,7)	3149	
34	$[t_4, 6_1 t_2]$	2336	(0,0)	2338	2358	106	$3_1 4_1 t_0$	3160	(0,6)	3160	3161
35	$5_1 8_1 t_0$	2337	(0,0)	2338	2338	107	$7_4 t_1$	3165	(2,3)	3164	
36	$6_1 7_2 t_0$	2358	(0,1)	2359	2361	109	$4_1 t_3$	3166	(0,2)	3171	
37	$6_1 7_1 t_1$	2366	(0,0)	2368	2369	110	$6_1 8_2 t_0$	3166	(0,3)	3166	
39	$[5_1 6_1 t_0]$	2401	(0,0)	2405	2406	111	$5_1 7_3 t_0$	3189	(1,3)	3192	
40	$3_1 7_1 t_0$	2404	(0,0)	2402	2402	112	$5_1 7_2 t_1$	3204	(1,2)	3209	
41	$[3_1 t_1, 4_1 8_1 t_0]$	2414	(0,0)	2418	2420	114	$4_1 7_1 t_2$	3223	(0,1)	3226	
42	$4_1 8_1 t_0$	2417	(0,0)	2416	2415	115	$[5_2 7_1 t_0, 5_1 7_1 t_2]$	3229	(2,1)	3235	
43	$3_1 t_1$	2426	(0,0)	2427	2420	117	$6_2 8_1 t_0$	3234	(1,2)	3232	
49	$7_4 t_0$	2517	(1,3)	2517		119	$[5_2 t_1]$	3247	(0,1)	3255	
50	$7_3 t_1$	2530	(0,1)	2531	[2543]	120	$4_1 7_3 t_0$	3263	(1,3)	3264	
51	$5_1 7_2 t_0$	2558	(0,1)	2561	2568	121	$t_6$	3267	(0,1)	3295	
53	$5_1 7_1 t_1$	2575	(0,0)	2579	2579	122	$4_1 7_2 t_1$	3280	(0,2)	3283	
54	$4_1 t_2$	2597	(0,0)	2598	2600	123	$8_2 t_2$	3285	(1,2)	3290	
55	$[5_2 t_0, 5_1 t_2]$	2604	(0,0)	2608	2608	124	$6_3 t_0$	3291	(1,3)	3289	3292
56	$4_1 7_2 t_0$	2633	(0,1)	2634	2636	126	$[4_1 5_1 7_1 t_0]$	3301	(0,1)	3305	
57	$4_1 7_1 t_1$	2650	(0,0)	2653	2652	127	$[4_1 5_1 t_1]$	3318	(0,1)	3322	
59	$4_1 5_1 t_0$	2676	(0,0)	2678	2678	128	$7_2 8_2 t_0$	3320	(2,3)	3320	3321
60	$7_1 8_2 t_0$	2690	(0,1)	2692	2690	130	$7_1 8_2 t_1$	3331	(1,3)	3335	
61	$8_2 t_1$	2703	(0,1)	2707	2702	131	$[8_1 t_4, 7_1 8_2 t_1, 8_2 t_2]$	3337	(1,2)	3340	
63	$4_2 t_0$	2746	(0,0)	2747	2746	132	$5_1 8_2 t_0$	3365	(1,2)	3368	
64	$6_1 7_1 8_1 t_0$	2764	(0,1)	2763	2764	133	$[8_1 t_4, 6_1 8_1 t_2]$	3370	(1,2)	3374	
65	$6_1 8_1 t_1$	2772	(0,1)	2773	2771	134	$4_2 7_1 t_0$	3372	(0,1)	3373	
66	$t_5$	2804	(0,0)	2818		135	$[6_1 t_4]$	3383	(1,2)	3386	
69	$3_1 8_1 t_0$	2810	(0,0)	2810	2810	136	$6_1 7_2 8_1 t_0$	3391	(2,2)	3389	
70	$8_1 t_3$	2826	(0,1)	2830	2834	138	$4_2 t_1$	3393	(0,3)	3396	

TABLE III. *Trans*-HCOOH. (Table II continued, CVPT [30], ICPH [28].)

# <sup>a</sup>	Assign. <sup>b</sup>	$\tilde{\nu}$	$(\delta_{10}, \delta_8)^c$	CVPT	ICPH	# <sup>a</sup>	Assign. <sup>b</sup>	$\tilde{\nu}$	$(\delta_{10}, \delta_8)^c$	CVPT	ICPH
140	6 <sub>1</sub> 7 <sub>1</sub> 8 <sub>1</sub> t <sub>1</sub>	3400	(1,3)	3399		198	[4 <sub>1</sub> t <sub>4</sub> ]	3705	(0,1)	3712	
141	[7 <sub>1</sub> t <sub>5</sub> ]	3430	(1,1)	3448		199	3 <sub>1</sub> 5 <sub>1</sub> 7 <sub>1</sub> t <sub>0</sub>	3706	(0,1)	3708	
142	3 <sub>1</sub> 7 <sub>1</sub> 8 <sub>1</sub> t <sub>0</sub>	3430	(0,1)	3431		200	[5 <sub>1</sub> 7 <sub>1</sub> t <sub>3</sub> , 7 <sub>1</sub> t <sub>5</sub> ]	3706	(1,2)	3707	
143	[6 <sub>1</sub> t <sub>4</sub> , 6 <sub>2</sub> t <sub>2</sub> ]	3433	(1,2)	3433		201	4 <sub>1</sub> 5 <sub>1</sub> 8 <sub>1</sub> t <sub>0</sub>	3711	(1,2)	3713	
144	[5 <sub>1</sub> 6 <sub>1</sub> 8 <sub>1</sub> t <sub>0</sub> ]	3434	(1,2)	3434		202	7 <sub>1</sub> 8 <sub>3</sub> t <sub>0</sub>	3717	(2,5)	3719	
145	3 <sub>1</sub> 8 <sub>1</sub> t <sub>1</sub>	3445	(0,1)	3447		204	4 <sub>1</sub> 6 <sub>1</sub> 7 <sub>2</sub> t <sub>0</sub>	3730	(2,1)	3729	
146	4 <sub>1</sub> 8 <sub>2</sub> t <sub>0</sub>	3451	(1,2)	3452		205	8 <sub>3</sub> t <sub>1</sub>	3730	(2,4)	3735	
147	6 <sub>2</sub> 7 <sub>2</sub> t <sub>0</sub>	3453	(2,4)	3450		206	3 <sub>1</sub> 5 <sub>1</sub> t <sub>1</sub>	3730	(0,5)	3732	
149	[6 <sub>2</sub> 7 <sub>1</sub> t <sub>1</sub> ]	3458	(1,2)	3461		207	4 <sub>1</sub> 6 <sub>1</sub> 7 <sub>1</sub> t <sub>1</sub>	3743	(1,2)	3745	
150	[7 <sub>1</sub> 8 <sub>1</sub> t <sub>3</sub> ]	3458	(1,3)	3461		208	[7 <sub>4</sub> t <sub>2</sub> ]	3745	(4,10)	3744	
154	[5 <sub>1</sub> 6 <sub>2</sub> t <sub>0</sub> ]	3490	(1,2)	3491		213	[4 <sub>1</sub> 5 <sub>1</sub> 6 <sub>1</sub> t <sub>0</sub> ]	3764	(1,2)	3770	
155	3 <sub>1</sub> 6 <sub>1</sub> 7 <sub>1</sub> t <sub>0</sub>	3504	(0,1)	3503		214	[5 <sub>3</sub> t <sub>0</sub> ]	3777	(1,2)	3785	
156	[3 <sub>1</sub> 6 <sub>1</sub> t <sub>1</sub> , 7 <sub>2</sub> 8 <sub>1</sub> t <sub>2</sub> ]	3511	(1,2)	3514		215	3 <sub>1</sub> 4 <sub>1</sub> 7 <sub>1</sub> t <sub>0</sub>	3781	(0,1)	3781	
157	[4 <sub>1</sub> 6 <sub>1</sub> 8 <sub>1</sub> t <sub>0</sub> ]	3512	(1,3)	3511		216	4 <sub>2</sub> 8 <sub>1</sub> t <sub>0</sub>	3784	(0,2)	3785	
158	[4 <sub>1</sub> 6 <sub>1</sub> 8 <sub>1</sub> t <sub>0</sub> ]	3515	(1,2)	3514		217	[4 <sub>1</sub> 7 <sub>1</sub> t <sub>3</sub> ]	3792	(2,1)	3797	
159	[3 <sub>1</sub> 6 <sub>1</sub> t <sub>1</sub> , 6 <sub>1</sub> 7 <sub>1</sub> t <sub>3</sub> ]	3522	(1,2)	3514		218	6 <sub>1</sub> 7 <sub>1</sub> 8 <sub>2</sub> t <sub>0</sub>	3793	(2,6)	3790	
161	[5 <sub>2</sub> 8 <sub>1</sub> t <sub>0</sub> ]	3536	(1,2)	3539		219	6 <sub>1</sub> 8 <sub>2</sub> t <sub>1</sub>	3801	(9,5)	3801	
162	3 <sub>2</sub> t <sub>0</sub>	3546	(0,0)	3545	3547	220	7 <sub>5</sub> t <sub>1</sub>	3805	(6,2)	3797	
163	7 <sub>4</sub> 8 <sub>1</sub> t <sub>0</sub>	3556	(4,5)	3550		221	3 <sub>1</sub> 4 <sub>1</sub> t <sub>1</sub>	3805	(6,11)	3807	
164	[7 <sub>2</sub> t <sub>4</sub> ]	3557	(1,9)	3564		222	7 <sub>6</sub> t <sub>0</sub>	3808	(3,14)	3783	
165	[4 <sub>1</sub> 6 <sub>2</sub> t <sub>0</sub> ]	3563	(1,3)			225	[5 <sub>1</sub> 7 <sub>4</sub> t <sub>0</sub> ]	3825	(5,10)	3825	
166	2 <sub>1</sub> 7 <sub>1</sub> t <sub>0</sub>	3566	(1,3)	3568	3566	227	3 <sub>1</sub> 8 <sub>2</sub> t <sub>0</sub>	3833	(1,4)	3835	3833
167	7 <sub>3</sub> 8 <sub>1</sub> t <sub>1</sub>	3567	(1,2)	3565		229	4 <sub>2</sub> 6 <sub>1</sub> t <sub>0</sub>	3835	(1,8)	3835	3836
168	3 <sub>1</sub> t <sub>3</sub>	3568	(0,4)	3570		230	[5 <sub>1</sub> 7 <sub>3</sub> t <sub>1</sub> ]	3837	(2,9)	3841	
169	4 <sub>1</sub> 6 <sub>2</sub> t <sub>0</sub>	3571	(1,2)	3565		234	6 <sub>2</sub> 7 <sub>1</sub> 8 <sub>1</sub> t <sub>0</sub>	3858	(3,5)	3854	
170	1 <sub>1</sub> t <sub>0</sub>	3576	(0,0)	3576	3575	235	[8 <sub>2</sub> t <sub>3</sub> ]	3859	(2,5)	3864	
171	2 <sub>1</sub> t <sub>1</sub>	3578	(0,0)	3581	3579	237	[6 <sub>2</sub> 8 <sub>1</sub> t <sub>1</sub> ]	3865	(2,4)	3854	
173	[6 <sub>1</sub> 7 <sub>2</sub> t <sub>2</sub> , 7 <sub>2</sub> t <sub>4</sub> ]	3588	(1,3)	3592		239	[5 <sub>2</sub> 7 <sub>1</sub> t <sub>1</sub> ]	3873	(1,3)	3884	
174	5 <sub>1</sub> 7 <sub>2</sub> 8 <sub>1</sub> t <sub>0</sub>	3592	(2,4)	3593		240	[6 <sub>1</sub> t <sub>5</sub> ]	3882	(1,3)	3890	
178	[5 <sub>1</sub> 7 <sub>1</sub> 8 <sub>1</sub> t <sub>1</sub> ]	3607	(1,4)	3611		247	4 <sub>1</sub> 7 <sub>4</sub> t <sub>0</sub>	3898	(1,8)	3895	
179	[5 <sub>1</sub> t <sub>4</sub> , 5 <sub>2</sub> 6 <sub>1</sub> t <sub>0</sub> ]	3612	(1,2)	3615		249	3 <sub>1</sub> 6 <sub>1</sub> 8 <sub>1</sub> t <sub>0</sub>	3911	(1,2)	3909	
180	6 <sub>1</sub> 7 <sub>4</sub> t <sub>0</sub>	3622	(6,4)	3615		250	4 <sub>1</sub> 7 <sub>3</sub> t <sub>1</sub>	3913	(2,5)	3914	
181	3 <sub>1</sub> 7 <sub>1</sub> t <sub>2</sub>	3625	(0,9)	3626		251	[7 <sub>1</sub> 8 <sub>2</sub> t <sub>2</sub> , 5 <sub>1</sub> 7 <sub>1</sub> 8 <sub>2</sub> t <sub>0</sub> ]	3914	(3,4)	3916	
182	6 <sub>1</sub> 7 <sub>3</sub> t <sub>1</sub>	3627	(3,9)	3625		254	[6 <sub>3</sub> t <sub>1</sub> ]	3918	(2,6)	3919	
183	[4 <sub>1</sub> 8 <sub>1</sub> t <sub>2</sub> ]	3634	(1,3)	3636		255	[6 <sub>1</sub> 8 <sub>1</sub> t <sub>3</sub> ]	3928	(2,4)	3929	
184	[4 <sub>1</sub> 5 <sub>1</sub> 8 <sub>1</sub> t <sub>0</sub> ]	3635	(1,5)	3638		256	[4 <sub>1</sub> 5 <sub>1</sub> 7 <sub>2</sub> t <sub>0</sub> ]	3930	(1,4)	3934	
185	3 <sub>1</sub> 7 <sub>3</sub> t <sub>0</sub>	3649	(1,4)	3649		257	[4 <sub>1</sub> 5 <sub>1</sub> 7 <sub>1</sub> t <sub>1</sub> ]	3944	(1,2)	3951	
186	[5 <sub>1</sub> 6 <sub>1</sub> 7 <sub>2</sub> t <sub>0</sub> ]	3656	(2,5)	3656		258	2 <sub>1</sub> 8 <sub>1</sub> t <sub>0</sub>	3952	(3,1)	3954	3952
187	[5 <sub>1</sub> 6 <sub>1</sub> 7 <sub>1</sub> t <sub>1</sub> , 6 <sub>1</sub> 7 <sub>1</sub> t <sub>3</sub> ]	3659	(1,3)			260	7 <sub>3</sub> 8 <sub>2</sub> t <sub>0</sub>	3955	(3,3)	3949	
189	3 <sub>1</sub> 7 <sub>2</sub> t <sub>1</sub>	3664	(1,2)	3664		262	[4 <sub>2</sub> t <sub>2</sub> , 4 <sub>2</sub> 5 <sub>1</sub> t <sub>0</sub> ]	3959	(0,7)	3965	
190	[4 <sub>1</sub> t <sub>4</sub> ]	3672	(1,1)	3670		263	[7 <sub>2</sub> 8 <sub>2</sub> t <sub>1</sub> ]	3962	(3,7)	3963	
191	4 <sub>1</sub> 7 <sub>2</sub> 8 <sub>1</sub> t <sub>0</sub>	3672	(1,4)	3672		264	[4 <sub>1</sub> 5 <sub>2</sub> t <sub>0</sub> , 4 <sub>2</sub> t <sub>2</sub> ]	3965	(1,6)	3977	
192	t <sub>7</sub>	3679	(1,2)			265	[7 <sub>2</sub> 8 <sub>2</sub> t <sub>1</sub> ]	3969	(3,8)	3963	
194	[7 <sub>3</sub> t <sub>3</sub> ]	3687	(1,3)	3688		266	3 <sub>1</sub> 6 <sub>2</sub> t <sub>0</sub>	3978	(1,2)	3975	3978
195	4 <sub>1</sub> 7 <sub>1</sub> 8 <sub>1</sub> t <sub>1</sub>	3688	(1,3)	3690		268	[6 <sub>2</sub> t <sub>3</sub> ]	3985	(2,4)	3984	
196	[5 <sub>1</sub> 6 <sub>1</sub> t <sub>2</sub> ]	3693	(1,2)	3698		269	5 <sub>1</sub> 7 <sub>1</sub> 8 <sub>2</sub> t <sub>0</sub>	3993	(3,6)	3994	

<sup>a</sup> #: Number of the state in the full vibrational energy list including *cis*, *trans*, and *delocalized* states.

<sup>b</sup> Excitation number for the rc-normal modes, 1<sub>n</sub>, 2<sub>n</sub>, 3<sub>n</sub>, 4<sub>n</sub>, 5<sub>n</sub>, 6<sub>n</sub>, 7<sub>n</sub>, 8<sub>n</sub> ( $n = 0, 1, \dots$ ), zero excitation is not shown. For the 9th degree of freedom, the type of torsional function (Fig. 11) and the excitation number is indicated,  $t_n/c_n/d_n$  with  $n \geq 0$ . ‘[...]’ labels the largest contribution(s) from strongly mixed states. The symmetry behaviour with respect to plane reflection can be derived from the properties of the 1D basis functions according to Table I by multiplication of the characters.

<sup>c</sup>  $(\delta_{10}, \delta_8) = (\tilde{\nu}_{b=9} - \tilde{\nu}_{b=10}, \tilde{\nu}_{b=8} - \tilde{\nu}_{b=9})$  is shown for assessment of the convergence. The reported  $\tilde{\nu}$  values and the assignment correspond to the  $b = 9$  basis set.

TABLE IV. *Cis*-HCOOH (including contributions from *trans* and *delocalized* states): vibrational energies,  $\tilde{\nu}$  in  $\text{cm}^{-1}$  referenced to the *trans*-ZPVE, computed with the GENIUSH-Smolyak approach in comparison with the internal-coordinate reaction-path Hamiltonian (ICPH) results [28]. (The footnotes are below Table V.)

# <sup>a</sup>	Assign. <sup>b</sup>	$\tilde{\nu}$	$(\delta_{10}, \delta_8)^c$	ICPH	# <sup>a</sup>	Assign. <sup>b</sup>	$\tilde{\nu}$	$(\delta_{10}, \delta_8)^c$	ICPH
11	ZPV- $c_0$	1418	(0,0)	1412	245	[c-t mixed]	3897	(3,2)	
21	$c_1$	1908	(0,0)	1904	246	[c+t mixed]	3898	(1,4)	
27	$7_1c_0$	2076	(0,0)	2080	248	$[5_1c_3, 6_1c_3]$	3902	(2,10)	[3915]
38	$c_2$	2372	(0,0)	2400	252	$[c_6-t \text{ mixed}, d_0]$	3914	(2,5)	
44	$8_1c_0$	2439	(0,1)	2450	253	$[c_6+t \text{ mixed}, d_0]$	3916	(2,7)	
48	$5_1c_0$	2514	(0,0)	2514	259	$8_2c_1$	3953	(2,4)	
52	$7_1c_1$	2568	(0,1)	2577	261	$4_17_1c_1$	3956	(2,4)	
58	$6_1c_0$	2665	(0,1)	2667	267	$[7_3c_0, 6_17_2c_0]$	3980	(2,8)	
62	$7_2c_0$	2733	(1,1)	2759	276	$[5_18_1c_1, 6_18_1c_1]$	4027	(3,5)	
67	$4_1c_0$	2807	(0,0)	2806	277	$[6_1c_3+3_18_1t_2]$	4029	(3,7)	
68	$c_3$	2809	(1,1)		278	$[6_1c_3-3_18_1t_2]$	4029	(2,7)	
78	$8_1c_1$	2931	(1,2)	2937	281	$[d_2, c, t \text{ mixed}]$	4036	(2,7)	
87	$5_1c_1$	3005	(1,1)	3009 <sup>†</sup>	283	$4_16_1c_0$	4049	(1,2)	4061
90	$7_1c_2$	3034	(1,1)		286	$7_4c_0$	4054	(2,8)	
99	$7_18_1c_0$	3098	(1,1)	3133	299	$[5_16_1c_1, 5_2c_1]$	4096	(2,9)	
104	$6_1c_1$	3149	(1,3)	3159 <sup>†</sup>	306	$7_18_2c_0$	4116	(2,7)	
108	$[5_17_1c_0, 6_17_1c_0]$	3166	(1,2)	3179	312	$[5_17_1c_2, 6_17_1c_2]$	4135	(2,3)	
113	$c_4$	3215	(1,1)		314	$7_2c_3$	4142	(4,6)	
116	$7_2c_1$	3229	(0,2)		321	$4_2c_0$	4166	(0,2)	4170
118	$3_1c_0$	3239	(0,0)	3235	324	$[6_18_1c_1, 5_18_1c_1]$	4178	(1,3)	
125	$4_1c_1$	3296	(0,1)	3299	327	$[5_17_18_1c_0, 6_17_18_1c_0]$	4187	(3,5)	
129	$[6_17_1c_0]$	3321	(1,3)		328	$3_1c_2$	4189	(2,4)	
137	$7_3c_0$	3391	(1,4)		329	[c, t mixed]	4189	(1,4)	
139	$8_1c_2$	3398	(1,4)		332	$4_1c_3$	4192	(2,5)	
148	$8_2c_0$	3455	(1,4)	3486	349	$[6_2c_1, 5_2c_1]$	4243	(5,11)	
151	$4_17_1c_0$	3465	(0,1)	3475	350	$[7_1c_5, 8_1c_4]$	4247	(2,7)	
152	$5_1c_2$	3467	(1,3)	3638	352	$[5_16_17_1c_0, 5_27_1c_0]$	4250	(1,7)	
153	$7_1c_3$	3473	(1,4)		353	$3_18_1c_0$	4254	(1,3)	4274
160	$5_18_1c_0$	3531	(1,2)	3536	355	$[7_28_1c_1-4_16_1t_3]$	4259	(4,4)	
172	$c_5$	3582	(2,2)	3570 <sup>*,†</sup>	356	$[7_28_1c_1+4_16_1t_3]$	4259	(4,9)	
175	$7_18_1c_1$	3594	(3,3)		357	$[7_1c_5, 8_1c_4]$	4260	(3,8)	
176	$[5_16_1c_0, 5_2c_0]$	3601	(1,3)	3595 <sup>†</sup>	362	$[6_17_1c_2, 7_2c_2]$	4273	(10,10)	
177	$[6_1c_2, 5_1c_2]$	3605	(2,6)	3638	369	$2_1c_0$	4291	(1,10)	4292
188	$[5_17_1c_1, 7_18_1c_1]$	3661	(2,3)		372	[c, t mixed]	4299	(1,8)	
193	$6_18_1c_0$	3686	(2,3)	3715 <sup>†</sup>	374	$[5_1c_4, 6_1c_4]$	4303	(2,13)	
197	$7_2c_2$	3698	(4,4)		380	$[5_17_2c_1, 6_17_2c_2]$	4320	(3,9)	
203	$3_1c_1$	3727	(0,1)	3733	383	[c, t mixed]	4325	(2,7)	
209	$[6_2c_0, 5_2c_0]$	3753	(2,4)	3761 <sup>*,†</sup>	384	$4_18_1c_1$	4325	(2,7)	
210	$4_1c_2-[t \text{ mixed}]$	3757	(2,2)		387	$[3_15_1c_0, 3_16_1c_0]$	4330	(1,4)	4322
211	$4_1c_2+[t \text{ mixed}]$	3757	(1,4)		391	$[6_17_18_1c_0, 7_28_1c_0]$	4346	(4,10)	
212	$7_28_1c_0$	3758	(1,6)		398	$7_3c_2$	4366	(5,12)	
223	$6_17_1c_1$	3811	(5,14)		399	$[d_3, c, t \text{ mixed}]$	4371	(5,9)	
224	$[5_17_2c_0, 6_17_2c_0]$	3820	(2,15)		404	$[6_2c_1, 5_16_1c_1]$	4378	(2,7)	
226	[c, t mixed]	3833	(2,4)		405	$3_17_1c_1$	4382	(2,6)	
228	$4_18_1c_0$	3833	(1,4)	3854	407	$[3_17_1c_1, 4_15_1c_1]$	4388	(5,3)	
231	$[8_1c_3, 8_1t_5]$	3842	(2,12)		416	$[6_27_1c_0, 5_17_2c_0]$	4408	(5,10)	
232	[c+t mixed]	3850	(1,7)		419	[c-t mixed]	4420	(4,5)	
233	[c-t mixed]	3854	(1,4)		420	[c+t mixed]	4420	(3,9)	
236	[c, t mixed]	3860	(2,5)		421	$4_17_1c_2$	4421	(4,10)	
238	[c, t mixed]	3873	(1,2)		422	$7_38_1c_0$	4423	(5,10)	
241	$7_1c_4$	3883	(2,6)		424	$8_2c_2$	4427	(-,9)	
242	$[3_17_1c_0, 4_15_1c_0]$	3890	(2,2)		437	$8_3c_0$	4467	(-,8)	
243	$7_3c_1$	3891	(3,4)		441	$[7_3c_1, 6_17_2c_1]$	4477	(-,12)	
244	$[3_17_1c_0, 6_2c_0]$	3892	(2,7)	3908	444	$[5_27_2c_0, 6_17_3c_0, 5_17_3c_0]$	4479	(-,15)	

TABLE V. *Cis*-HCOOH (including contributions from *trans* and *delocalized* states). (Table IV continued, ICPH [28].)

# <sup>a</sup>	Assign. <sup>b</sup>	$\tilde{\nu}$	$(\delta_{10}, \delta_8)^c$	ICPH	# <sup>a</sup>	Assign. <sup>b</sup>	$\tilde{\nu}$	$(\delta_{10}, \delta_8)^c$	ICPH
446	[3 <sub>1</sub> 6 <sub>1</sub> c <sub>0</sub> ]	4483	(-,16)	4496	492	[7 <sub>1</sub> c <sub>6</sub> ,c,d,t mixed]	4583	(-,8)	
447	[c+t mixed]	4485	(-,14)		496	[4 <sub>1</sub> c <sub>4</sub> +3 <sub>1</sub> 6 <sub>2</sub> 7 <sub>1</sub> t <sub>0</sub> ]	4596	(-,7)	
448	[c-t mixed]	4490	(-,12)		497	[4 <sub>1</sub> c <sub>4</sub> -3 <sub>1</sub> 6 <sub>2</sub> 7 <sub>1</sub> t <sub>0</sub> ]	4597	(-,7)	
452	4 <sub>1</sub> 7 <sub>1</sub> 8 <sub>1</sub> c <sub>0</sub>	4493	(-,17)		498	4 <sub>1</sub> c <sub>4</sub>	4598	(-,7)	
453	[5 <sub>1</sub> 8 <sub>1</sub> c <sub>2</sub> ,6 <sub>1</sub> 8 <sub>1</sub> c <sub>2</sub> ]	4495	(-,17)		508	4 <sub>1</sub> 7 <sub>2</sub> c <sub>1</sub>	4618	(-,9)	
454	[c,t mixed]	4496	(-,19)		509	[5 <sub>2</sub> 8 <sub>1</sub> c <sub>0</sub> ,5 <sub>1</sub> 6 <sub>1</sub> 8 <sub>1</sub> c <sub>0</sub> ]	4619	(-,8)	
456	[c,t mixed]	4506	(-,15)		510	7 <sub>1</sub> 8 <sub>2</sub> c <sub>1</sub>	4620	(-,15)	
459	[7 <sub>1</sub> 8 <sub>1</sub> c <sub>3</sub> +5 <sub>1</sub> t <sub>6</sub> ]	4514	(-,12)		511	3 <sub>1</sub> 4 <sub>1</sub> c <sub>0</sub>	4622	(-,15)	4626
460	[7 <sub>1</sub> 8 <sub>1</sub> c <sub>3</sub> -5 <sub>1</sub> t <sub>6</sub> ]	4518	(-,10)		512	3 <sub>1</sub> c <sub>3</sub>	4622	(-,14)	
465	[c,t mixed]	4529	(-,8)		515	[8 <sub>1</sub> c <sub>5</sub> -4 <sub>1</sub> t <sub>6</sub> ]	4629	(-,18)	
467	[4 <sub>1</sub> 6 <sub>1</sub> c <sub>1</sub> ]	4534	(-,8)		517	[8 <sub>1</sub> c <sub>5</sub> +4 <sub>1</sub> t <sub>6</sub> ]	4637	(-,12)	
470	[3 <sub>1</sub> 7 <sub>2</sub> c <sub>0</sub> ]	4543	(-,11)		520	[6 <sub>1</sub> 8 <sub>1</sub> c <sub>2</sub> ]	4643	(-,10)	
472	5 <sub>1</sub> 8 <sub>2</sub> c <sub>0</sub>	4546	(-,10)		524	[7 <sub>4</sub> c <sub>0</sub> ,6 <sub>1</sub> 7 <sub>3</sub> c <sub>0</sub> ,5 <sub>1</sub> 6 <sub>1</sub> 7 <sub>2</sub> c <sub>0</sub> ]	4646	(-,11)	
476	[3 <sub>1</sub> 7 <sub>2</sub> c <sub>0</sub> -6 <sub>3</sub> 7 <sub>2</sub> t <sub>0</sub> ]	4550	(-,15)		527	4 <sub>2</sub> c <sub>1</sub>	4654	(-,7)	4672
477	[3 <sub>1</sub> 7 <sub>2</sub> c <sub>0</sub> +6 <sub>3</sub> 7 <sub>2</sub> t <sub>0</sub> ]	4550	(-,16)		535	[5 <sub>1</sub> c <sub>5</sub> ]	4671	(-,7)	
479	[7 <sub>2</sub> c <sub>4</sub> ]	4553	(-,17)		542	[5 <sub>3</sub> c <sub>0</sub> ,5 <sub>2</sub> 6 <sub>1</sub> c <sub>0</sub> ]	4684	(-,17)	
480	[7 <sub>2</sub> c <sub>4</sub> ]	4553	(-,16)		544	[5 <sub>1</sub> 7 <sub>1</sub> 8 <sub>1</sub> c <sub>1</sub> ,6 <sub>1</sub> 7 <sub>1</sub> 8 <sub>1</sub> c <sub>2</sub> ]	4689	(-,15)	
481	[5 <sub>1</sub> 6 <sub>1</sub> c <sub>2</sub> ]	4557	(-,16)		547	[c,t mixed]	4697	(-,14)	
484	7 <sub>4</sub> c <sub>1</sub>	4564	(-,16)		549	[c,t mixed]	4702	(-,12)	
485	[5 <sub>1</sub> 6 <sub>7</sub> 1c <sub>3</sub> ,6 <sub>1</sub> 7 <sub>1</sub> c <sub>3</sub> ]	4565	(-,16)		550	[c,t mixed]	4702	(-,12)	

<sup>a,b,c</sup> see footnotes to Fig. III.

<sup>†</sup>: Revised assignment based on the Supplementary Material of Ref. [28].

\*: Tentative comparison.

TABLE VI. *Delocalized*-HCOOH: selected vibrationally excited states computed with the GENIUSH-Smolyak approach ( $b = 9$ ) with significant contribution from delocalized torsional basis functions,  $d_0$ ,  $d_1$ ,  $d_2$ , and  $d_3$ . The vibrational energy,  $\tilde{\nu}$  in  $\text{cm}^{-1}$ , is referenced to the *trans*-ZPVE.

# <sup>a</sup>	Dominant basis-state contributions <sup>b</sup>				$\tilde{\nu}$	$(\delta_{10}, \delta_8)^c$
252	-0.56 6 <sub>3</sub> 7 <sub>1</sub> t <sub>0</sub>	+0.32 6 <sub>4</sub> 7 <sub>1</sub> t <sub>0</sub>	... +0.20 c <sub>6</sub>	+0.15 d <sub>0</sub>	3914	(2,5)
253	+0.44 c <sub>6</sub>	+0.37 d <sub>0</sub>	-0.33 7 <sub>1</sub> t <sub>6</sub>		3916	(2,7)
281	-0.36 d <sub>1</sub>	+0.32 5 <sub>1</sub> t <sub>5</sub>			4036	(2,7)
284	+0.34 6 <sub>2</sub> 7 <sub>1</sub> t <sub>2</sub>	+0.32 d <sub>0</sub>	-0.30 6 <sub>1</sub> 7 <sub>1</sub> t <sub>4</sub>		4053	(5,4)
287	+0.41 d <sub>0</sub>	+0.33 7 <sub>1</sub> t <sub>6</sub>	+0.31 5 <sub>1</sub> 6 <sub>1</sub> 7 <sub>1</sub> 8 <sub>1</sub> t <sub>0</sub>		4060	(2,5)
303	+0.41 d <sub>1</sub>	+0.30 3 <sub>1</sub> 5 <sub>1</sub> 8 <sub>1</sub> t <sub>0</sub> +0.27 5 <sub>2</sub> 6 <sub>1</sub> t <sub>1</sub>		-0.25 6 <sub>1</sub> t <sub>3</sub>	4112	(2,4)
309	+0.47 d <sub>1</sub>	-0.27 5 <sub>1</sub> 6 <sub>2</sub> t <sub>1</sub>	-0.27 5 <sub>2</sub> 6 <sub>1</sub> t <sub>1</sub>		4125	(2,4)
376	-0.33 5 <sub>3</sub> t <sub>1</sub>	+0.30 d <sub>2</sub>	+0.30 5 <sub>1</sub> 6 <sub>1</sub> t <sub>3</sub>		4311	(2,10)
389	+0.42 4 <sub>1</sub> 5 <sub>1</sub> 7 <sub>1</sub> 8 <sub>1</sub> t <sub>0</sub> +0.25 4 <sub>1</sub> 7 <sub>1</sub> 8 <sub>1</sub> t <sub>2</sub> +0.21 d <sub>2</sub>				4340	(2,6)
399	+0.55 d <sub>3</sub>	+0.22 3 <sub>1</sub> 4 <sub>1</sub> t <sub>2</sub>	+0.21 6 <sub>1</sub> t <sub>6</sub>		4371	(4,9)

<sup>a,b,c</sup> see footnotes to Fig. III.



## VII. SUMMARY, CONCLUSION, AND OUTLOOK

Variational vibrational excitation energies have been reported for the formic acid molecule up to ca. 4700  $\text{cm}^{-1}$ , which is slightly beyond the top of the *cis-trans* isomerization barrier, using system-adapted curvilinear coordinates in the GENIUSH-Smolyak approach developed in the present work and a high-level *ab initio* potential energy surface (PES) taken from Ref. [28].

The results confirm (within 1–5  $\text{cm}^{-1}$ ) up to 2500  $\text{cm}^{-1}$ , and improve (by 5–10  $\text{cm}^{-1}$ ) between 2500 and 4000  $\text{cm}^{-1}$  the 6th-order canonical van Vleck perturbation theory (CVPT) energies [30] that were obtained from a computation localized on the *trans* PES well. Both the *cis* and *trans* energies computed with the GENIUSH-Smolyak approach are in an overall good agreement, but improve (by 10–40  $\text{cm}^{-1}$ ) upon the internal-coordinate path Hamiltonian (ICPH) results that similarly to the present work account for both the *cis* and *trans* wells of the PES. There exists another potential energy surface and multi-configuration time-dependent Hartree (MCTDH) computations have been reported using that PES [29, 46]. Direct comparison with those results have not been reported in this work, because our current focus was on the development of a computational procedure that can be used to provide benchmark quality vibrational energies up to and possibly beyond the isomerization barrier of the formic acid molecule. We think that we have almost achieved this goal, further necessary work with larger basis sets and an improved basis pruning condition is in progress and results will be reported in future work.

Already in the present paper, *cis-trans* entangled states, corresponding ‘tunneling splittings’, and the (*cis* or *trans*) localized to *delocalized* transition taking place near the top barrier were shortly discussed. Benchmark quality computed data (limited by the quality of the PES) on these interesting features will become available soon with the outlined theoretical, computational progress. We are not aware of detailed experimental data of these phenomena in HCOOH, and we look forward to developments from the experimental side.

## ACKNOWLEDGMENT

We thank the financial support of the Swiss National Science Foundation (PROMYS Grant, No. IZ11Z0\_166525). The authors are indebted to Tucker Carrington, Attila Császár, and their co-workers for joint work and discussions over the past decade that had resulted in ideas and developments necessary to accomplish the present research. We also thank Martin Suhm and Arman Nejad who made us interested in working on this system.

- 
- [1] D. Lauvergnat and A. Nauts, Exact numerical computation of a kinetic energy operator in curvilinear coordinates, *J. Chem. Phys.* **116**, 8560 (2002).
  - [2] E. Mátyus, G. Czakó, and A. G. Császár, Toward black-box-type full- and reduced-dimensional variational (ro)vibrational computations, *J. Chem. Phys.* **130**, 134112 (2009).
  - [3] C. Fábri, E. Mátyus, and A. G. Császár, Rotating full- and reduced-dimensional quantum chemical models of molecules, *J. Chem. Phys.* **134**, 074105 (2011).
  - [4] C. Fábri, E. Mátyus, and A. G. Császár, Numerically constructed internal-coordinate Hamiltonian with Eckart embedding and its application for the inversion tunneling of ammonia, *Spectrochim. Acta* **119**, 84 (2014).
  - [5] A. Yachmenev and S. N. Yurchenko, Automatic differentiation method for numerical construction of the rotational-vibrational Hamiltonian as a power series in the curvilinear internal coordinates using the Eckart frame, *J. Chem. Phys.* **143**, 014105 (2015).
  - [6] D. Lauvergnat and A. Nauts, Quantum dynamics with sparse grids: A combination of Smolyak scheme and cubature. Application to methanol in full dimensionality, *Spectrochim. Acta* **119**, 18 (2014).
  - [7] A. Nauts and D. Lauvergnat, Numerical on-the-fly implementation of the action of the kinetic energy operator on a vibrational wave function: application to methanol, *Mol. Phys.* **116**, 3701 (2018).
  - [8] X.-G. Wang and T. Carrington Jr, Using monomer vibrational wavefunctions to compute numerically exact (12D) rovibrational levels of water dimer, *J. Chem. Phys.* **148**, 074108 (2018).
  - [9] X.-G. Wang and T. Carrington, A variational calculation of vibrational levels of vinyl radical, *J. Chem. Phys.* **152**, 204311 (2020).
  - [10] P. M. Felker and Z. Bačić, Weakly bound molecular dimers: Intramolecular vibrational fundamentals, overtones, and tunneling splittings from full-dimensional quantum calculations using compact con-

- tracted bases of intramolecular and low-energy rigid-monomer intermolecular eigenstates, *J. Chem. Phys.* **151**, 024305 (2019).
- [11] P. M. Felker and Z. Bačić, H<sub>2</sub>O–CO and D<sub>2</sub>O–CO complexes: Intra- and intermolecular rovibrational states from full-dimensional and fully coupled quantum calculations, *J. Chem. Phys.* **153**, 074107 (2020).
  - [12] Y. Liu, J. Li, P. M. Felker, and Z. Bačić, HCl–H<sub>2</sub>O dimer: an accurate full-dimensional potential energy surface and fully coupled quantum calculations of intra- and intermolecular vibrational states and frequency shifts, *Phys. Chem. Chem. Phys.* **23**, 7101 (2021).
  - [13] G. Avila and T. Carrington, Nonproduct quadrature grids for solving the vibrational Schrödinger equation, *J. Chem. Phys.* **131**, 174103 (2009).
  - [14] G. Avila and T. Carrington, Using nonproduct quadrature grids to solve the vibrational Schrödinger equation in 12D, *J. Chem. Phys.* **134**, 054126 (2011).
  - [15] G. Avila and T. Carrington, Using a pruned basis, a non-product quadrature grid, and the exact Watson normal-coordinate kinetic energy operator to solve the vibrational Schrödinger equation for C<sub>2</sub>H<sub>4</sub>, *J. Chem. Phys.* **135**, 064101 (2011).
  - [16] G. Avila and E. Mátyus, Toward breaking the curse of dimensionality in (ro)vibrational computations of molecular systems with multiple large-amplitude motions, *J. Chem. Phys.* **150**, 174107 (2019).
  - [17] G. Avila and E. Mátyus, Full-dimensional (12D) variational vibrational states of CH<sub>4</sub>·F<sup>−</sup>: Interplay of anharmonicity and tunneling, *J. Chem. Phys.* **151**, 154301 (2019).
  - [18] A. Chen and D. Lauvergnat, ElVibRot-MPI: parallel quantum dynamics with Smolyak algorithm for general molecular simulation, arXiv preprint arXiv:2111.13655 (2021).
  - [19] R. Wodraszka and T. Carrington Jr, A pruned collocation-based multiconfiguration time-dependent Hartree approach using a Smolyak grid for solving the Schrödinger equation with a general potential energy surface, *J. Chem. Phys.* **150**, 154108 (2019).
  - [20] R. Wodraszka and T. Carrington, A rectangular collocation multi-configuration time-dependent Hartree (MCTDH) approach with time-independent points for calculations on general potential energy surfaces, *J. Chem. Phys.* **154**, 114107 (2021).
  - [21] T. Carrington, Using collocation to study the vibrational dynamics of molecules, *Spectrochim. Acta* **248**, 119158 (2021).
  - [22] D. Peláez, K. Sadri, and H.-D. Meyer, Full-dimensional MCTDH/MGPF study of the ground and lowest lying vibrational states of the bihydroxide H<sub>3</sub>O<sub>2</sub><sup>−</sup> complex, *Spectrochim. Acta* **119**, 42 (2014).
  - [23] F. Otto, Y.-C. Chiang, and D. Peláez, Accuracy of Potfit-based potential representations and its impact on the performance of (ML-)MCTDH, *Chem. Phys.* **509**, 116 (2018).
  - [24] R. L. Panadés-Barrueta and D. Peláez, Low-rank sum-of-products finite-basis-representation (SOP-FBR) of potential energy surfaces, *J. Chem. Phys.* **153**, 234110 (2020).
  - [25] T. Halverson and B. Poirier, Large scale exact quantum dynamics calculations: Ten thousand quantum states of acetonitrile, *Chem. Phys. Lett.* **624**, 37 (2015).
  - [26] T. Halverson and B. Poirier, One Million Quantum States of Benzene, *J. Phys. Chem. A* **119**, 12417 (2015).
  - [27] J. Sarka and B. Poirier, Hitting the Trifecta: How to Simultaneously Push the Limits of Schrödinger Solution with Respect to System Size, Convergence Accuracy, and Number of Computed States, *J. Chem. Theory Comput.* **17**, 7732 (2021).
  - [28] D. P. Tew and W. Mizukami, Ab initio Vibrational Spectroscopy of *cis*- and *trans*-Formic Acid from a Global Potential Energy Surface, *J. Phys. Chem. A* **120**, 9815 (2016).
  - [29] F. Richter and P. Carbonnière, Vibrational treatment of the formic acid double minimum case in valence coordinates, *J. Chem. Phys.* **148**, 064303 (2018).
  - [30] A. Nejad and E. L. Sibert, The Raman jet spectrum of *trans*-formic acid and its deuterated isotopologs: Combining theory and experiment to extend the vibrational database, *J. Chem. Phys.* **154**, 064301 (2021).
  - [31] E. B. Wilson, Jr., J. C. Decius, and P. C. Cross, *Molecular Vibrations: The Theory of Infrared and Raman Vibrational Spectra*, Dover Publications, Inc., New York (1980).
  - [32] Wolfram Research, Inc., Mathematica, Version 12.1, Champaign, IL, 2020.
  - [33] D. Papoušek and M. R. Aliev, *Molecular vibrational-rotational spectra* (1982).
  - [34] J. Sarka, A. G. Császár, S. C. Althorpe, D. J. Wales, and E. Mátyus, Rovibrational transitions of the methane–water dimer from intermolecular quantum dynamical computations, *Phys. Chem. Chem. Phys.* **18**, 22816 (2016).
  - [35] J. Sarka, A. G. Császár, and E. Mátyus, Rovibrational quantum dynamical computations for deuterated isotopologues of the methane–water dimer, *Phys. Chem. Chem. Phys.* **19**, 15335 (2017).
  - [36] D. Ferenc and E. Mátyus, Bound and unbound rovibrational states of the methane–argon dimer, *Mol. Phys.* **117**, 1694 (2019).
  - [37] A. Martín Santa Daría, G. Avila, and E. Mátyus, Performance of a black-box-type rovibrational method in comparison with a tailor-made approach: Case study for the methane–water dimer, *J. Chem. Phys.* **154**, 224302 (2021).

- [38] A. Martín Santa Daría, G. Avila, and E. Mátyus, Fingerprint region of the formic acid dimer: variational vibrational computations in curvilinear coordinates, *Phys. Chem. Chem. Phys.* **23**, 6526 (2021).
- [39] J. C. Light and T. Carrington Jr., Discrete-Variable Representations and their Utilization, in *Adv. Chem. Phys.* (John Wiley & Sons, Ltd, 2000) Chap. 14, pp. 263–310.
- [40] G. Avila, D. Papp, G. Czakó, and E. Mátyus, Exact quantum dynamics background of dispersion interactions: case study for CH<sub>4</sub>·Ar in full (12) dimensions, *Phys. Chem. Chem. Phys.* **22**, 2792 (2020).
- [41] S. A. Smolyak, Quadrature and interpolation formulas for tensor products of certain classes of functions, in *Doklady Akademii Nauk*, Vol. 148 (Russian Academy of Sciences, 1963) pp. 1042–1045.
- [42] F. Heiss and V. Winschel, Likelihood approximation by numerical integration on sparse grids, *J. Economet.* **144**, 62 (2008).
- [43] M. J. Bramley and T. Carrington Jr, Calculation of triatomic vibrational eigenstates: Product or contracted basis sets, Lanczos or conventional eigensolvers? What is the most efficient combination?, *J. Chem. Phys.* **101**, 8494 (1994).
- [44] X.-G. Wang and T. Carrington Jr, A finite basis representation Lanczos calculation of the bend energy levels of methane, *J. Chem. Phys.* **118**, 6946 (2003).
- [45] T. Carrington Jr and X.-G. Wang, Computing ro-vibrational spectra of van der Waals molecules, *Wiley Interdis. Rev.: Comp. Mol. Sci.* **1**, 952 (2011).
- [46] A. Aerts, P. Carbonnière, F. Richter, and A. Brown, Vibrational states of deuterated *trans*- and *cis*-formic acid: DCOOH, HCOOD, and DCOOD, *J. Chem. Phys.* **152**, 024305 (2020).

## SUPPLEMENTARY MATERIAL

TABLE VII. Curvilinear normal coordinate ( $\xi_i$ ) parameters for the *trans* formic acid and the  $\tilde{\nu}^{\text{HO}}$  harmonic frequencies in  $\text{cm}^{-1}$ .  $\xi_i = \xi_i^{(\text{eq})} + \sum_{j=1}^8 Q_j \mathcal{L}_{i,j}$ . The units correspond to bohr for the distances and radian for the angles.

		$Q_1$	$Q_2$	$Q_3$	$Q_4$	$Q_5$	$Q_6$	$Q_7$	$Q_8$
$\tilde{\nu}^{\text{HO}}$		3765.35	3089.16	1816.23	1412.08	1323.08	1140.45	1102.9	631.798
	$\xi^{(\text{eq})}$	$\mathcal{L}_{i,j}$ :							
$r_1$	2.53601	-0.00160774	-0.00280096	-0.02092050	0.00377681	0.02909350	-0.05012370	0.00000000	-0.01130860
$r_2$	2.26578	0.00010330	-0.00563876	0.05024730	0.01044820	-0.00463876	-0.00645253	0.00000000	-0.00125626
$r_3$	2.06736	-0.00179791	0.10827700	0.00275970	0.00264300	0.00228843	0.00062604	0.00000000	-0.00061152
$r_4$	1.82737	0.09711080	0.00200363	-0.00081998	0.00186474	-0.00447978	-0.00239879	0.00000000	0.00087992
$\theta_1$	2.17992	0.00180103	0.00647238	-0.00956847	-0.00088388	-0.02380230	0.01197050	0.00000000	-0.04093320
$\theta_2$	1.91986	-0.00193900	-0.00262074	0.03055210	-0.06940420	-0.01605430	-0.01774360	0.00000000	0.02458280
$\theta_3$	1.86227	-0.00028928	-0.00389619	0.02221480	-0.02777300	0.06806850	0.05177930	0.00000000	-0.02681930
$\tau_1$	0.00000	0.00000000	0.00000000	0.00000000	0.00000000	0.00000000	0.00000000	0.12015200	0.00000000

TABLE VIII. Curvilinear normal coordinate ( $\xi_i$ ) parameters for the *cis* formic acid and the  $\tilde{\nu}^{\text{HO}}$  harmonic frequencies in  $\text{cm}^{-1}$ .  $\xi_i = \xi_i^{(\text{eq})} + \sum_{j=1}^8 Q_j \mathcal{L}_{i,j}$ . The units correspond to bohr for the distances and radian for the angles.

		$Q_1$	$Q_2$	$Q_3$	$Q_4$	$Q_5$	$Q_6$	$Q_7$	$Q_8$
$\tilde{\nu}^{\text{HO}}$		3826.32	3006.92	1861.52	1428.97	1300.17	1125.37	1040.96	664.495
	$\xi^{(\text{eq})}$	$\mathcal{L}_{i,j}$ :							
$r_1$	2.54924	-0.00208335	-0.00284458	-0.01799320	0.00497105	0.03407310	-0.04825930	0.00000000	-0.01260780
$r_2$	2.25255	0.00036668	-0.00571702	0.04977190	0.00837307	-0.00669357	-0.00607253	0.00000000	-0.00269151
$r_3$	2.07870	-0.00213001	0.10972700	0.00329455	0.00295397	0.00078314	0.00230952	0.00000000	-0.00087318
$r_4$	1.81792	0.09636670	0.00240434	-0.00130866	0.00061663	-0.00231159	-0.00001521	0.00000000	0.00012556
$\theta_1$	2.13454	0.00179629	0.00633024	-0.00979878	-0.00421724	-0.01876390	0.01536720	0.00000000	-0.04226280
$\theta_2$	1.98444	-0.00175648	-0.00257378	0.02977090	-0.07143720	-0.00623438	-0.01340060	0.00000000	0.02285910
$\theta_3$	1.90590	-0.00118818	-0.00387435	0.02117820	-0.01419170	0.08259160	0.03606030	0.00000000	-0.02161040
$\tau_1$	0.00000	0.00000000	0.00000000	0.00000000	0.00000000	0.00000000	0.00000000	0.12498000	0.00000000